INTERNATIONAL JOURNAL OF CLIMATOLOGY
Int. J. Climatol. **20**: 1285–1327 (2000)

ENSO AND CLIMATIC SIGNALS ACROSS THE INDIAN OCEAN BASIN IN THE GLOBAL CONTEXT: PART I, INTERANNUAL COMPOSITE PATTERNS

C.J.C. REASON[a,*], R.J. ALLAN[b], J.A. LINDESAY[c] and T.J. ANSELL[a]

[a] *School of Earth Sciences, University of Melbourne, Parkville, Victoria, Australia*
[b] *CSIRO Division of Atmospheric Research, PMB 1, Mordialloc, Victoria, Australia*
[c] *Department of Geography, Australian National University, Canberra, A.C.T., Australia*

Received 2 November 1998
Revised 22 November 1999
Accepted 26 November 1999

ABSTRACT

This study focuses on the interplay between mean sea level pressure (MSLP), sea surface temperature (SST), and wind and cloudiness anomalies over the Indian Ocean in seasonal composite sequences prior to, during, and after strong, near-global El Niño and La Niña episodes. It then examines MSLP and SST anomalies in the 2–2.5-year quasi-biennial (QB) and 2.5–7-year low-frequency (LF) bands that carry the bulk of the raw ENSO signal. Finally, these fields were examined in conjunction with patterns of correlations between rainfall and joint spatiotemporal empirical orthogonal function (EOF) time series band pass filtered in the QB and LF bands.

The seasonal composites indicate that the El Niño-1 (La Niña-1) pattern tends to display a more robust and coherent (weaker and less organized) structure during the evolution towards the mature stage of the event. The reverse tends to be apparent in the cessation period after the peak phase of an event, when El Niño events tend to collapse quite quickly.

Climatic variables over the Indian Ocean Basin linked to El Niño and La Niña events show responses varying from simultaneous, to about one season's lag. In general, SSTs tend to evolve in response to changes in cloud cover and wind strength over both the north and south Indian Ocean. There are also strong indications that the ascending (descending) branch of the Walker circulation is found over the African continent (central Indian Ocean) during La Niña phases, and that the opposite configuration occurs in El Niño events. These alternations are linked to distinct warm–cool (cool–warm) patterns in the north–south SST dipole over the western Indian Ocean region during the El Niño (La Niña) events.

An examination of MSLP and SST anomaly patterns in the QB and LF bands shows that signals are more consistent during El Niño-1 and El Niño sequences than they are during La Niña-1 and La Niña sequences. The QB band has a tendency to display the opposite anomaly patterns to that seen on the LF band during the early stages of event onset, and later stage of event cessation, during both El Niño–Southern Oscillation (ENSO) phases. El Niño events tend to be reinforced by signals on both bands up to their mature phase, but are then seen to erode rapidly, as a result of the presence of distinct La Niña anomalies on the QB band after their peak phase. During La Niña events, the opposite is observed during their cessation phase.

Both QB and LF bands often display SST dipole anomalies that are not clearly evident in the raw composites alone. An eastern Indian Ocean SST dipole shows a tendency to occur during the onset phase of particular El Niño or La Niña episodes, especially during the austral autumn–winter (boreal spring–summer) and, when linked to tropical-temperate cloud bands, can influence Australian rainfall patterns.

Analyses of seasonal correlations between rainfall and joint MSLP and SST EOF time series on QB and LF bands and their dynamical relationship with MSLP and SST anomalies during El Niño and La Niña events, show that the interplay between atmospheric circulation and SST anomalies dictates the observed rainfall response. Instances where either, or both, QB and LF bands are the prime influence on observed rainfall regimes are evident. This ability to discriminate the finer structure of physical relationships, correlations and patterns provides a deeper insight into Indian Ocean responses to ENSO phases. Copyright © 2000 Royal Meteorological Society.

KEY WORDS: ENSO; Indian Ocean; climatic variability

* Correspondence to: School of Earth Sciences, University of Melbourne, Parkville, Victoria 3010, Australia; e-mail: cjr@met.unimelb.edu.au/cjr@egs.uct.ac.za

1. INTRODUCTION

One of the most prominent examples of climatic variability is that associated with El Niño–Southern Oscillation (ENSO) events. Most scientific research on ENSO has focused on the Pacific Ocean Basin where the core of the physical processes underlying the phenomenon occur (Allan *et al*., 1996). ENSO impacts on rainfall and temperature around the Indian Ocean Basin have been detailed in Ropelewski and Halpert (1987, 1989) and Halpert and Ropelewski (1992), but little emphasis has been given to the physical signatures of ENSO across the Indian Ocean as a whole since the first general overviews by Cadet (1985), Reverdin *et al*. (1986) and Fu and Fletcher (1988).

Specific relationships between ENSO and climatic conditions in various countries bordering the Indian Ocean Basin continue to be examined. Efforts focusing on interannual modulation of rainfall patterns in India and Sri Lanka (e.g. Suppiah, 1988; Pan and Oort, 1990; Parthasarathy *et al*., 1991; Thapliyal and Kulshrestha, 1991; Parthasarathy *et al*., 1992; Vijayakumar and Kulkarni, 1995; Suppiah, 1996; Kripalani and Kulkarni, 1997a,b, 1998) and Africa (e.g. Lindesay *et al*., 1986; Nicholson and Entekhabi, 1986; Tyson, 1986; Wolter, 1987, 1989; Janowiak, 1988; Lindesay, 1988; van Heerden *et al*., 1988; Lindesay and Vogel, 1990; Matarira, 1990; Hutchinson, 1992; Hastenrath *et al*., 1993; Jury *et al*., 1993, 1996; Nicholson and Palao, 1993; Jury, 1994; Makarau and Jury, 1997; Nicholson, 1997; Nicholson and Kim, 1997; Rocha and Simmonds, 1997a,b; Reason, 1998; Reason and Lutjeharms, 1998) have been published in the last 15 years. Coherent, north–south-oriented interannual sea surface temperature (SST) dipole patterns in the western portion of the basin, both related, and apparently unrelated, to ENSO, have been investigated by researchers in southern Africa (e.g. Walker and Lindesay, 1989; Mason, 1990, 1995; Walker, 1990; Jury *et al*., 1996; Reason, 1999). In addition, there are ongoing concerns about ENSO, and other interannual fluctuations, modulating Indian Ocean SST patterns in the eastern portion of the basin, thus providing a different influence on Australian rainfall from that usually associated with the phenomena in the Pacific (Nicholls, 1989; Drosdowsky, 1993a,b; Smith, 1994; Allan *et al*., 1996), and the role of the oceanic 'throughflow' between the Pacific and Indian Oceans, via the Indonesian region (Wyrtki, 1987; Hirst and Godfrey, 1993, 1994; Clarke and Liu, 1994; Qu *et al*., 1994; Wajsowicz, 1994, 1995; Meyers, 1996; Reason *et al*., 1996b). Most recently, Saji *et al*. (1999) and Webster *et al*. (1999) propose an east–west-oriented equatorial Indian Ocean SST dipole pattern that modulates rainfall in East Africa and Indonesia, and suggest that this dipole operates independently of ENSO. This is contrary to the work of Chambers *et al*. (1999), who find a similar SST dipole but relate it to ENSO through the extension of the Indo-Australasian node of the Southern Oscillation component of ENSO into the Indian Ocean.

Studies are still debating the relationship between the Indian Monsoon system and the ENSO phenomenon, with indications that interactions might be 'selectively interactive', so that the ENSO signal (the Indian Monsoon) is only able to dominate over the Indian Monsoon (ENSO signal) during the boreal autumn–winter (spring–summer) half of the year (Webster and Yang, 1992; Webster, 1995). Such findings have been linked further to the long observed boreal spring (austral autumn) 'predictability barrier', and the collapse of persistence in ENSO characteristics (Webster, 1995; Torrence and Compo, 1998; Torrence and Webster, 1998, 1999). Other research has indicated the presence of decadal to multidecadal fluctuations in ENSO–Indian Monsoon interactions (e.g. Parthasarathy *et al*., 1991; Thapliyal and Kulshrestha, 1991; Vijayakumar and Kulkarni, 1995; Allan *et al*., 1996; Suppiah, 1996; Torrence and Webster, 1998, 1999), and distinct bidecadal variations in southern African rainfall (Tyson, 1986; Mason, 1990, 1995; Mason and Tyson, 1992). The wider patterns of lower frequency fluctuations in ENSO, and its climatic relationships across the Indian Ocean Basin, have been discussed in a number of papers, with specific studies of such variability and its causes having only recently received attention (Allan *et al*., 1995; Reason *et al*., 1996a,b, 1998a,b).

Apart from efforts to understand African rainfall modulations by tropical Atlantic and western Indian Ocean responses to ENSO (Nicholson, 1997; Nicholson and Kim, 1997), there has been no coherent focus on the ENSO signal across the region as a whole. In particular, it is not known whether suggested changes in the climatic regime and/or ENSO nature over the Pacific Ocean Basin since the mid-1970s (e.g.

Graham, 1994; Kerr, 1994; Miller *et al*., 1994a,b; Trenberth and Hurrell, 1994; Jiang *et al*., 1995; Kleeman *et al*., 1996; Latif *et al*., 1996, 1997) are also found to occur across the Indian Ocean region. This paper is part one of a detailed investigation of relationships between interannual ENSO and decadal to multidecadal variability, and their influence on climatic patterns and physical processes over the Indian Ocean Basin.

First, this study examines the nature of canonical patterns in atmospheric and oceanic variables over the region, as inferred by the 'classical' ENSO definition of a phenomenon operating in the 2–7-year time frame. The mechanisms by which Indian Ocean SST anomalies are generated and evolve during ENSO events have yet to be established firmly. For example, Godfrey *et al*. (1995) note that winds over the north Indian Ocean do not change much during ENSO events, and suggest that changes in cloudiness (e.g. Wright *et al*., 1985) may play a role in accounting for the SST anomalies. Godfrey *et al*. (1995) also note the possibility of changes in the intensity of the Indonesian 'throughflow' (Clarke and Liu, 1994; Meyers, 1996) contributing towards Indian Ocean SST anomalies. Model studies (e.g. Hirst and Godfrey, 1993, 1994; Reason *et al*., 1996b) indicate that the south Indian Ocean is sensitive to changes in the Indonesian 'throughflow', on time scales of several years and longer; whether there is also significant sensitivity on shorter time scales is not clear, however.

In an attempt to establish the relationships between mean sea level pressure (MSLP), SST, wind and cloud over the Indian Ocean region during ENSO events, a composite approach (e.g. Rasmusson and Carpenter, 1982) is initially adopted. The magnitude of the Southern Oscillation Index (SOI) and SST in the Niño-3 and Niño-4 regions has been used to identify so called El Niño-1, El Niño, La Niña-1, and La Niña years over the period of 1878–1989, and seasonal composites of these years are formed. The evolution of anomalies from the long-term mean for these seasonal composites is then examined for MSLP, SST, cloud cover, wind speed and direction. An appraisal of near-global MSLP data during an El Niño composite sequence using data for the period 1946–1993 (Harrison and Larkin, 1996), provides an important reference point for this part of the study.

Recent detailed analyses of climatic signals using joint empirical orthogonal function (EOF) and singular value decomposition (SVD) techniques to examine recently updated versions of the global mean sea level (GMSLP) and global sea-ice and sea surface temperature (GISST) data sets (Basnett and Parker, 1997; Folland *et al*., 1998) have revealed important structural aspects of the quasi-biennial (QB; 2–2.5-year) and low-frequency (LF) interannual (2.5–7-year) components of the ENSO signal (Allan, 2000). The results of this work show that much of what is observed about ENSO nature is the result of the phasing of the QB and LF elements of the phenomenon. Such interactions appear to be vital to any efforts aimed at improving our understanding of the boreal spring (austral autumn) 'predictability barrier' (Clarke *et al*., 1998), fluctuations in climatic impacts amongst various El Niño and La Niña events, and the distinct modulations of a number of the physical manifestations that occur in the environment during ENSO phases.

In the second part of this study, a re-examination of the composites of MSLP and SST in the ENSO QB and LF bands is performed (wind and cloud cover data were found to be too sparse to filter successfully). This is achieved by band pass filtering the raw MSLP and SST data in the significant QB and LF bands found in the spectral analysis of Allan (2000), and then re-compositing both of the filtered QB and LF data in El Niño-1, El Niño, La Niña-1, and La Niña years. Periods of 'protracted' El Niño (as in the first half of the 1990s) and 'protracted' La Niña events (as resolved in Allan and D'Arrigo, 1999) are not considered in the composites formulated in this part of the study. These are addressed in a second, complimentary paper, currently in preparation, which focuses on an examination of 'El Niño-like' and 'La Niña-like' episodes on much longer quasi-decadal and bidecadal time frames.

Resolution of the dominant signals and patterns in climatic variables does not, in itself, provide a complete picture of the degree of climatic impact involved in ENSO phases. Most studies have presented this information through the use of maps and diagrams showing relationships and correlations between climatic phenomena and variables, such as rainfall, temperature, streamflow etc. Such an approach has been employed most widely with regard to ENSO influence on both regional to global scale rainfall, and surface air temperature patterns (Ropelewski and Halpert, 1987, 1989; Kiladis and Diaz, 1989; Halpert

and Ropelewski, 1992; Allan *et al.*, 1996). A better understanding of the influence of ENSO phases on rainfall patterns is provided by simultaneous seasonal correlations between joint MSLP and SST EOF time series (Allan, 2000) and global land and island precipitation data (Hulme, 1992) band pass filtered in the QB and LF bands. The results of these correlations are shown in the final section of this paper. Overall, the three-stage approach used in this paper sheds more light on the nature, characteristics and impact of the phenomenon across the Indian Ocean Basin.

2. DATA AND METHODS

The data sets used in the study are comprised of the UKMO GISST, version 2.2 (Parker *et al.*, 1995; Rayner *et al.*, 1996), for SST, the UKMO/CSIRO GMSLP, version 2.1f, for MSLP (Allan *et al.*, 1996; Basnett and Parker, 1997), and the comprehensive ocean atmosphere data set (COADS) (Woodruff *et al.*, 1987) for winds and cloudiness. Allan *et al.* (1995, 1996) have provided a thorough discussion of both the quality of these data sets and the density of data sampling over this century for the Indian Ocean region, while Harrison and Larkin (1996) have done a raw composite analysis of El Niño evolution using near-global COADS MSLP data for the period of 1946–1993. Based on these analyses, it is felt that the above data sets represent the best that are currently available, and facilitate a composite study of the sort performed here. It should be noted that for the correlation analysis detailed in the final section of this paper, the GISST data set used is the most recent GISST 3.0 version of SST data released by the UKMO.

All of the data presented in this study are anomalies from the 1878–1989 base period. As in Allan *et al.* (1995), an objective spatial filter is used to provide some smoothing of the final fields of all but the GMSLP and GISST data (Hantel, 1970). In addition, all fields have been examined for statistical significance at the 95% level using a grid point t-test, and for field significance at the 95% level using Monte Carlo methods in a pool-permutation procedure (PPP) as employed by Allan *et al.* (1995). The t-tests assess the statistical significance of data at each grid point. All MSLP and SST anomaly composites show regions above the local 95% significant t-test levels. As cloudiness and wind anomaly composites have had to be spatially smoothed, they are less robust when examined for statistical significance, and no t-test results are shown.

In order to highlight the most important components of the ENSO signal over the Indian Ocean, a composite technique has been employed. This technique is similar to that of Rasmusson and Carpenter (1982), who focused mainly on the Pacific region, and involves seasonal composites formed from individual years, classified as El Niño-1, El Niño, La Niña-1, and La Niña (Table I). Only pronounced events were used in the composites, with the above classifications chosen on the basis of values of the SOI and SST anomalies in the central and eastern equatorial Pacific. Both 'protracted' El Niño and La Niña events that were resolved by this process are not used in the composites developed for this study. The composites are based on the 3-month seasons January–March (JFM), April–June (AMJ), July–September (JAS) and October–December (OND). As the major focus of this study is the ENSO signal in the Indian Ocean, including the waters south of both Africa and Australia, the composites which are relevant to the seasonal cycle of SST in the south Indian Ocean, and to the wet and dry seasons in tropical Australia and southern Africa, have been chosen, rather than those defined in the Pacific-oriented study of Rasmusson and Carpenter (1982).

In this spirit, attempts have only been made to link the evolution in SST, winds and cloud for the Indian Ocean region. Changes in these parameters with time are noted for the Pacific, particularly as they may relate to those occurring in the Indian Ocean, but the links between them or the complex atmosphere–ocean interactions that underpin the ENSO signal in the Pacific have not been considered. The latter is comprehensively dealt with in Philander (1990), with Allan *et al.* (1996) containing many references to more recent works in this area.

To examine the nature and structure of the ENSO signal more completely, the GMSLP and GISST data were band pass filtered in the 2–2.5-year (QB), and 2.5–7-year (LF) bands, following the confirmation of significant climatic signals in these frequency ranges in Allan (2000). A Chebychev filter

Table I. Years used in El Niño-1, El Niño, La Niña-1, and La Niña raw, and band pass filtered, QB and LF band composite seasonal sequences (shown in bold)

El Niño-1	El Niño	La Niña-1	La Niña
1877	**1878**	*1879*	*1880*
1888	**1889**	**1886**	**1887**
1896	*1897*	**1889**	**1890**
1899	**1900**	**1892**	**1893**
1902	**1903**	*1909*	*1910*
1905	**1906**	*1916*	*1917*
1911	*1912*	*1917*	*1918*
1913	*1914*	**1924**	**1925**
1914	*1915*	**1933**	**1934**
1918	**1919**	**1938**	**1939**
1925	**1926**	**1942**	**1943**
1930	**1931**	**1949**	**1950**
1940	*1941*	*1954*	*1955*
1941	*1942*	*1955*	*1956*
1957	**1958**	**1970**	**1971**
1963	**1964**	*1973*	*1974*
1965	**1966**	*1975*	*1976*
1972	**1973**	**1988**	**1989**
1982	**1983**		
1986	**1987**		
1990	*1993*		

Other 'protracted' El Niño and La Niña events to be examined in a subsequent paper are shown in italics.

(T. Fisher, 1998, personal communication) was used for this purpose. The spectra structure of the GMSLP and GISST data resolving these signals can be seen in Figure 1. Once filtered in the QB and LF bands, both variables were composited into El Niño-1, El Niño, La Niña-1, and La Niña years in the seasons defined earlier.

In the final section of the paper, the analysis of ENSO impacts is expanded to examine the relationship of the joint EOF time series in the QB and LF bands, found in the spatiotemporal analyses of MSLP and SST observations in Allan (2000) with the global rainfall data set of Hulme (1992; see comparison with other climatologies and discussions with regard to temporal and spatial sampling by Hulme and New, 1997) through simultaneous seasonal correlations over the period of 1900–1994.

3. RAW SEASONAL COMPOSITES OF MSLP, SST, WIND AND CLOUD ANOMALIES

3.1. El Niño-1

Indo-Pacific anomalies of MSLP, SST, wind speed, wind vector and cloud for each season of the El Niño-1 composite year are given in Figures 2 and 3**.** At the beginning of the sequence (JFM), weak positive MSLP anomalies are present over most of the Indian Ocean, except in the central south Indian Ocean region (Figure 2(a)), while warm SST exist throughout much of the eastern and central Pacific, with the beginnings of the horseshoe shaped anomaly evident in the central Pacific (Figure 3(a)). Elsewhere, almost the entire tropical and midlatitude ocean is cool. At this time, most of the Indian Ocean is characterized by positive wind anomalies (Figure 3(c)) with areas of enhanced southeasterly trades in the south Indian Ocean, and monsoonal flow in regions of the equatorial western and eastern Indian Ocean (Figure 3(c and d)). In terms of magnitude, these anomalies are somewhat smaller than those evident in the tropical Pacific. The Indian Ocean wind anomalies are consistent with a cooler ocean (Figure 3(c)), if SST there is being driven by enhanced surface fluxes, and mixing driven by the wind.

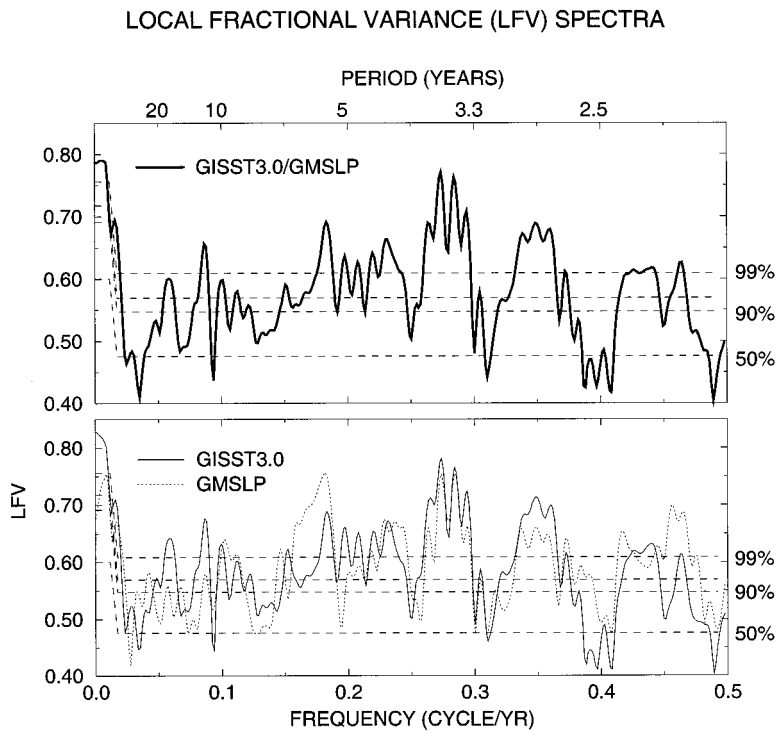

Figure 1. Multi-taper frequency-domain singular value decomposition (MTM-SVD) localized variance spectrum of (a) joint analysis of historical GISST 3.0 and GMSLP 2.1f, and (b) separate analyses of historical GISST 3.0 and GMSLP2.1f from 1871–1994 (relative variance is explained by the first eigen value of the SVD as a function of frequency). The 50, 90 and 99% statistical confidence limits are shown as horizontal lines, and various significant climatic features in the spectrum are pointed out on the diagram. In (b), the GISST 3.0 spectra is shown by the solid line and the GMSLP 2.1f spectra is shown by the dashed line (from Allan, 2000)

Large areas of the south Indian Ocean show increased cloud cover (Figure 3(b)), again consistent with cool conditions, if SST in that region are mainly responding to atmospheric changes, while much of the north Indian Ocean displays decreased cloud.

During AMJ, MSLP anomalies become organized into an El Niño structure across the Indo-Pacific domain (Figure 2(b)). Oceanic warming intensifies in the eastern and central tropical Pacific (Figure 4(a)) and regions of increased cloud, and anomalous westerly anomalies appear near, and east of, the dateline (Figure 4(b–d)), while the cool conditions over most of the Indian Ocean have weakened, and large patches of warm anomalies have appeared in the south Indian Ocean (Figure 4(a)). These south Indian Ocean warm anomaly areas partially coincide with regions of anomalously weaker winds (Figure 4(c and d)) and reduced cloud cover (Figure 4(b)), and more obviously with regions where the wind direction anomalies (Figure 4(d)) are associated with changes to the Ekman drift, and imply relative advection of warmer water and air into the warm SST anomaly region. Elsewhere, over the south Indian Ocean, there are mainly strong wind anomalies (Figure 4(c and d)), and increased cloud (Figure 4(b)), consistent with the cool SST anomalies. Some patches of strong wind anomalies exist in the north Indian Ocean, but most of this ocean displays weak wind anomalies and negative cloud anomalies (Figure 4(b–d)), thus, it is not clear that the SST anomalies here are responding to the atmospheric changes.

By JAS, the MSLP dipole (characteristic of El Niño conditions) is well-established (Figure 2(c)). Warm conditions have appeared over virtually the entire north Indian Ocean, as well as most of the south Indian Ocean, as the signal intensifies in the central and equatorial Pacific (Figure 5(a)), and significant increases in cloud and westerly wind anomalies (Figure 5(b–d)) are found between about 160°E and 135°W. Winds are weaker (Figure 5(c and d)) over large parts of the tropical western Indian Ocean, but it seems likely to be mainly the reduction in cloud cover (Figure 5(b)) that is associated with the warmer SST anomalies

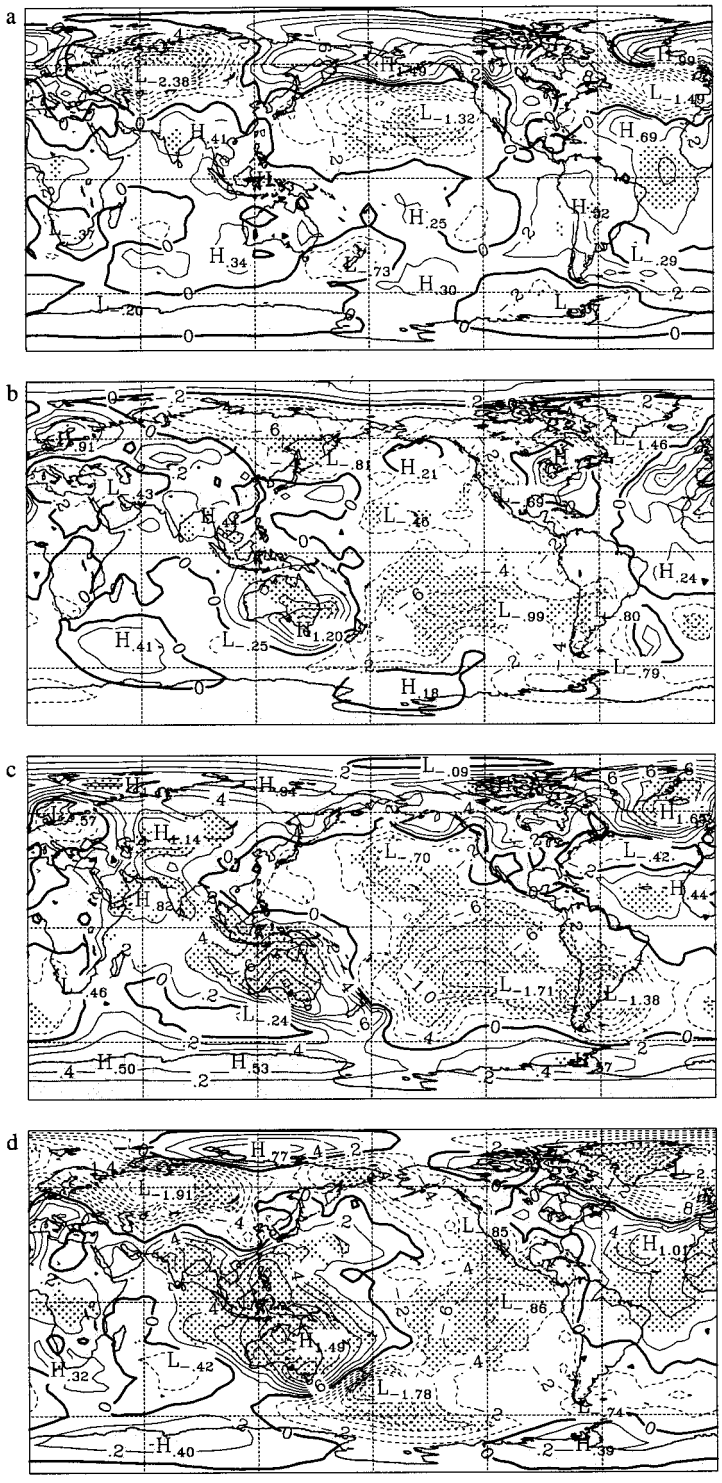

Figure 2. Raw MSLP seasonal El Niño-1 composite anomaly sequences for (a) JFM, (b) AMJ, (c) JAS, and (d) OND over the period 1878–1989. Dashed (solid) contours denote negative (positive) values. Events used in the composites are given in Table I. MSLP are in hPa (plotted every 0.2 hPa). Significant *t*-test areas at the 95% level are stippled

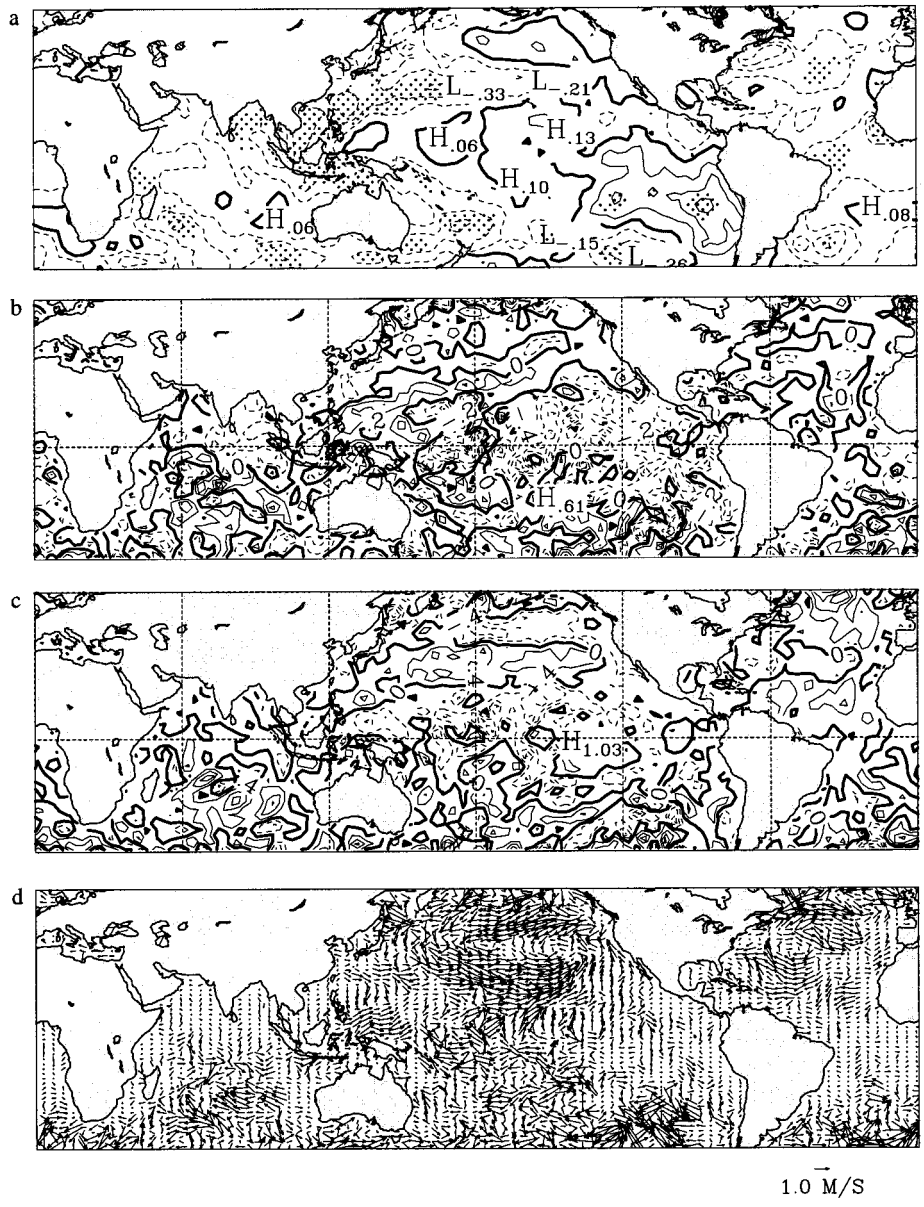

Figure 3. Raw JFM seasonal El Niño-1 composite anomaly sequences for (a) SST in °C (plotted every 0.1 °C with significant *t*-test areas at the 95% level stippled), (b) cloudiness values in oktas (plotted every 0.2 oktas), (c) scalar wind speed in ms^{-1} (plotted every 0.4 ms^{-1}), and (d) wind vectors in ms^{-1}, with a key to the vector lengths on the figure. Dashed (solid) contours denote negative (positive) values in (a), (b) and (c). Events used in the composites are given in Table I

over the north Indian Ocean and the central and western tropical south Indian Ocean. Reduced cloud and weaker winds (Figure 5(b–d)) also occur over parts of the cool region in the eastern south Indian Ocean. Godfrey *et al.* (1995) have suggested that changes in sea level and tidal mixing in the Indonesian region may be responsible for the cool SST, rather than any direct SST response here to cloud cover, or surface latent and sensible heat fluxes induced by areas of weaker winds. The other region of cool Indian Ocean SST anomalies is in the southern midlatitudes (Figure 5(a)). This zone has some regions of increased cloud anomalies (Figure 5(b)), which would be favourable for cool SST anomalies; however, most of the region shows weaker wind magnitudes (Figure 5(c)), which would tend to work in the opposite direction. It may

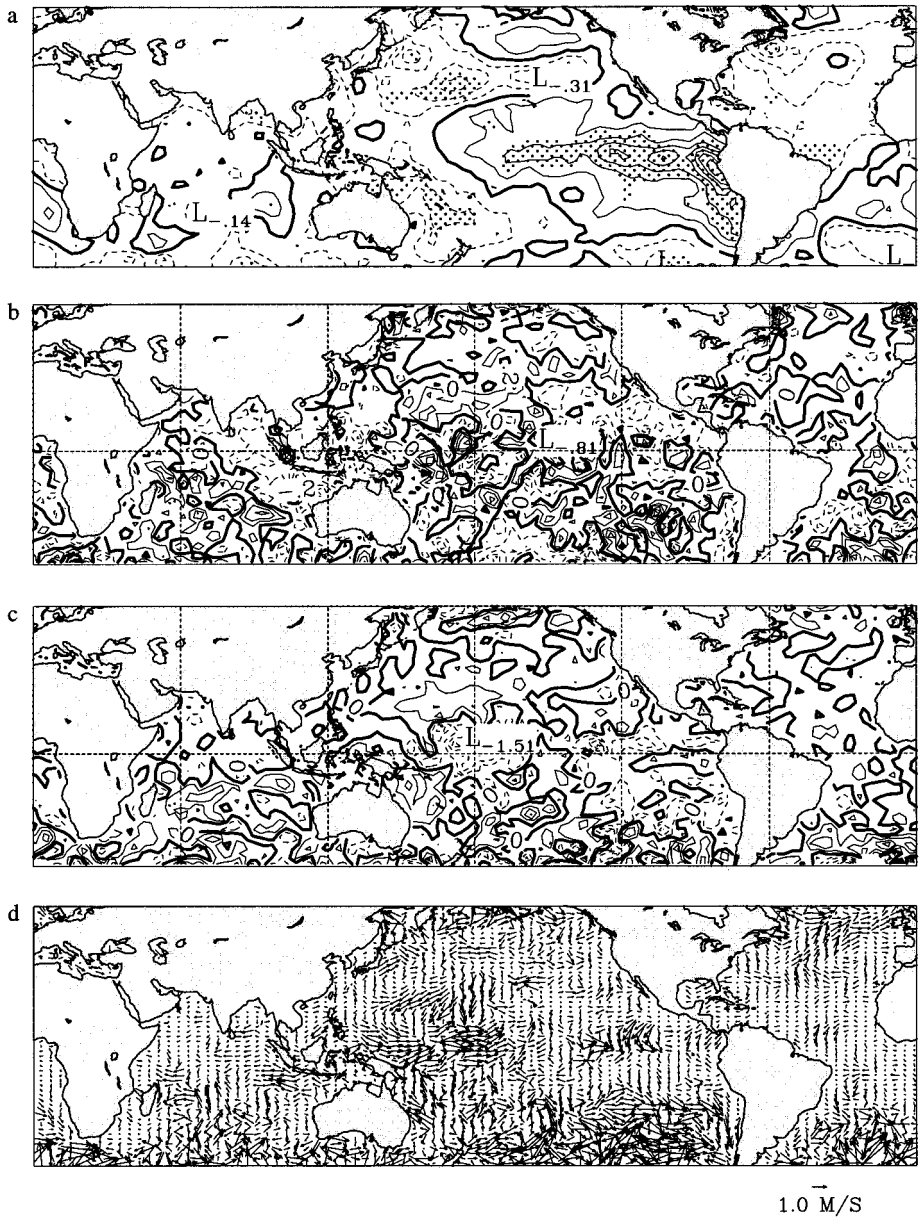

Figure 4. As in Figure 3, except for AMJ season

be that the relative direction of the wind changes (Figure 5(d)), being mainly westward, often with a southerly component, is such as to weaken the outflow of warm Agulhas waters east across the southern midlatitudes.

The following OND period sees major increases in cloud cover in the tropical Southern Hemisphere, and significantly strengthened positive MSLP anomalies over Australia, southeast Asia and the eastern Indian Ocean (Figure 2(d)). A less obvious strengthening can be seen across southern and eastern Africa, while there are negative MSLP anomalies over the tropics to midlatitudes of the western and central south Indian Ocean. This pattern of MSLP anomalies in the region from Africa to the central longitudes of the south Indian Ocean may reflect the apparent shift in the local Walker circulation, that often tends to occur during El Niño events (e.g. Lindesay, 1988). The SST pattern shows warm conditions over all the

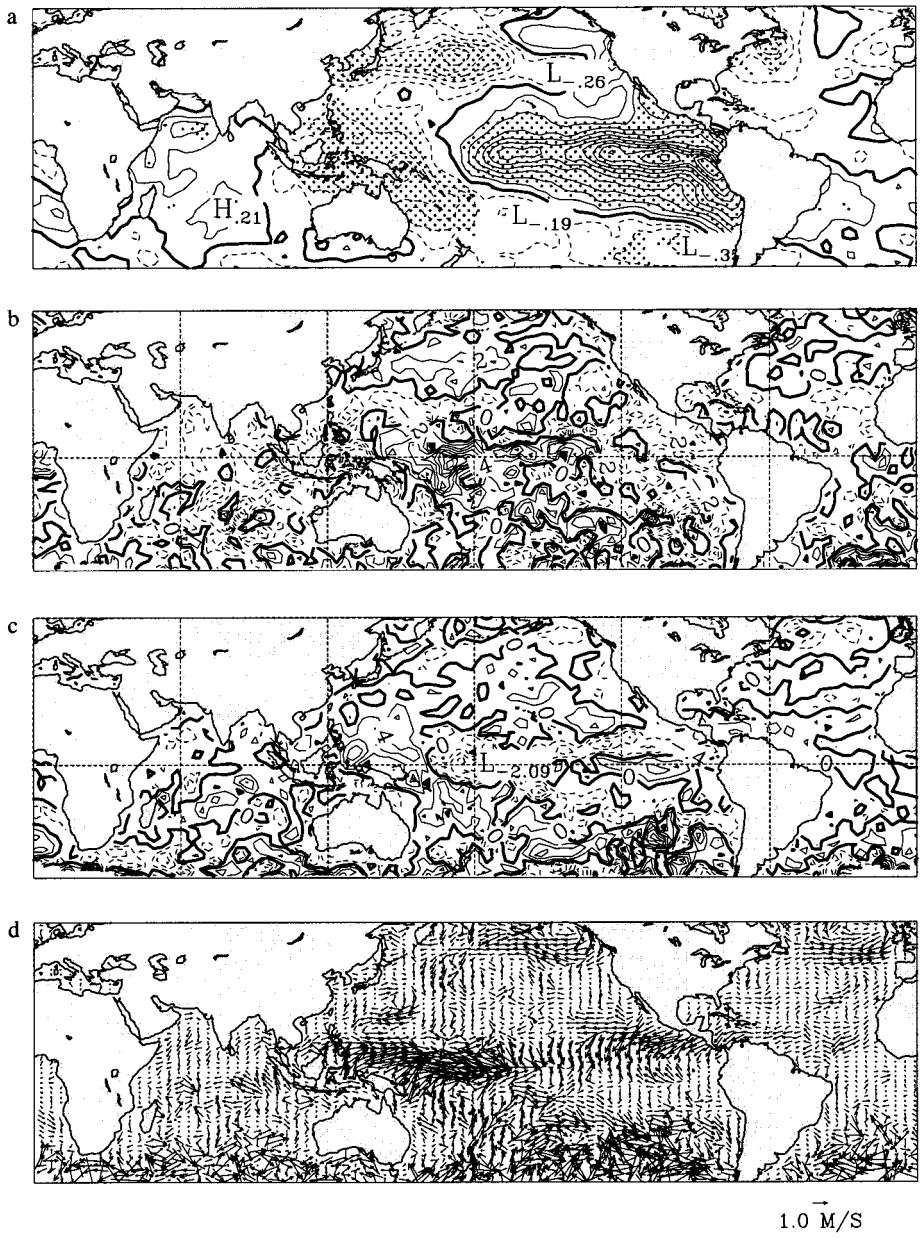

Figure 5. As in Figure 3, except for JAS season

Indian Ocean, excepting small areas of cool SST anomaly in the southern midlatitudes, and in the Timor Sea region (Figure 6(a)). At this time, the signal in the Pacific Ocean is near its peak (Figure 6(a)) in terms of both warm SST anomalies extending west of the Americas, to just west of the dateline, and increased cloud and anomalous tropical westerly anomalies over the region from 160°E to about 135°W. Weaker winds and reduced cloud (Figure 6(b–d), which are favourable for warmer SST anomalies, tend to be mainly concentrated in the eastern half of the Indian Ocean. The relative direction of the wind anomalies (Figure 6(d)) in the western half of the Indian Ocean would tend to favour warmer SST in some cases, however. For example, in the Arabian Sea region, the direction implies relative convergence of waters along the coast, and relative downwelling (on average upwelling tends to occur there at least until

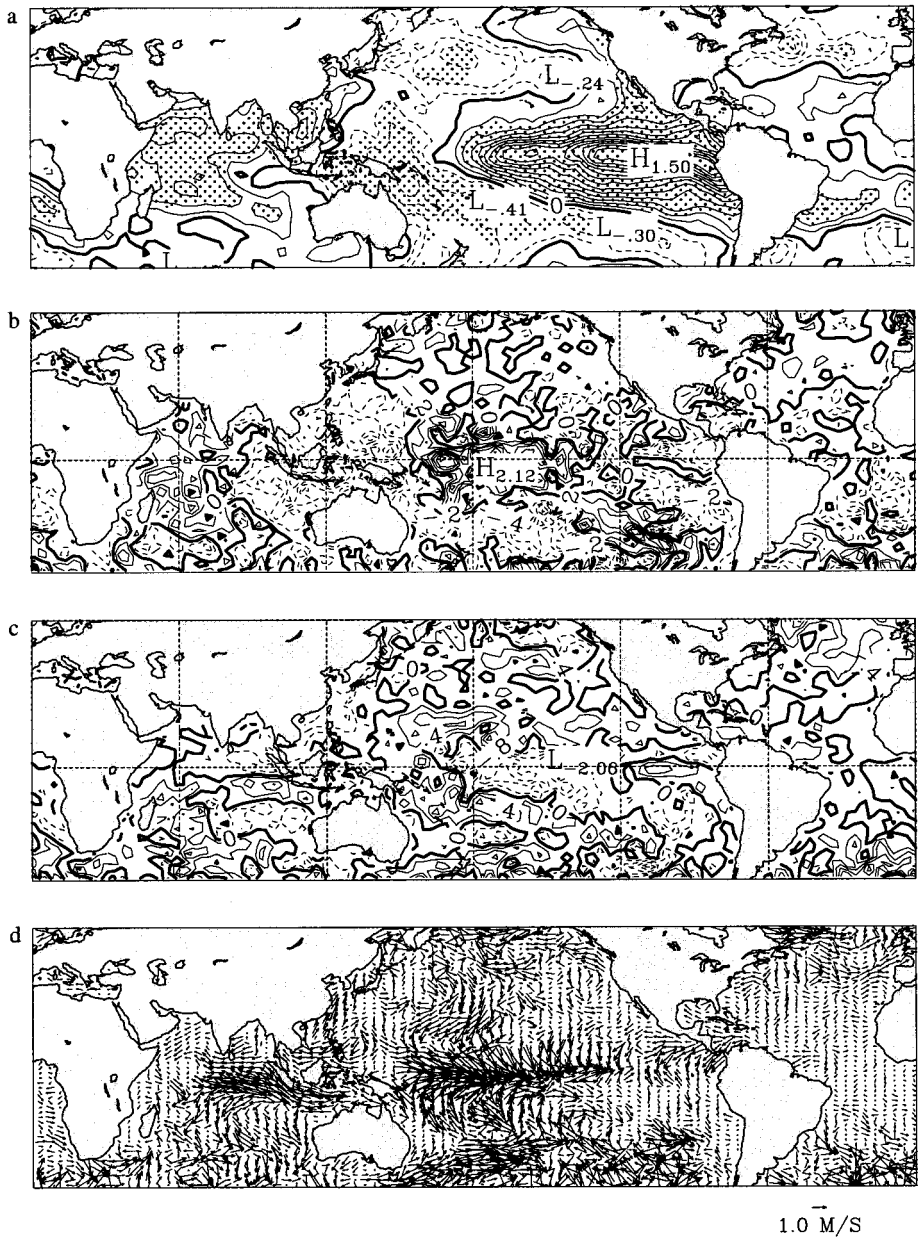

Figure 6. As in Figure 3, except for OND season

October). Similarly, north and east of Madagascar, and along the Tanzanian Coast, the anomalous wind directions are again favourable for relative downwelling. Further to the east, there are large regions of relative easterly and northeasterly wind changes (Figure 6(d)), which would imply relative Ekman drift of warmer waters southwards, as well as relative warm air advection.

In summary, the composite El Niño-1 year begins with mainly cool conditions in the Indian Ocean, and ends with mainly warm conditions across the basin. This warming of the tropical Indian Ocean appears to occur more or less at the same time in the north and south Indian Ocean, except for the Indonesian seas region, which lags behind by at least one seasonal period. Much, but not all, of the SST evolution appears to be associated with weaker winds and reduced cloud cover, which would favour warming if the

latter is mainly responding via latent and sensible heat fluxes and upper ocean mixing to the atmospheric changes. The atmospheric changes may reflect a shift and weakening, particularly during the Southern Hemisphere warm season (October–March), of the ascending branch of a Walker type circulation extending across the equatorial to tropical south Indian Ocean (e.g. Tyson, 1986; Lindesay, 1988). A shift in the ascending branch off tropical southern Africa to the western Indian Ocean may account for regions of increased cloud near Madagascar, evident during the JFM and OND periods of the composite (Figure 3(b) and Figure 6(b)). Being more dominated by the monsoonal reversal in atmospheric circulation, such a process is not obvious over the north Indian Ocean region. In terms of timing, the composite suggests that the signal in the tropical south Indian Ocean may evolve more quickly and coherently than that in the north Indian Ocean.

3.2. El Niño

During JFM of the El Niño composite (Figure 7(a)), positive MSLP anomalies are evident over almost all the region north of about 30–40°S, with negative anomalies in the southern midlatitudes. At this stage, the increase in MSLP over Australia is near its peak, and the region of positive MSLP anomalies in the global tropics outside the central to eastern Pacific is at its most spatially extensive. In addition, warm conditions in the central and eastern tropical Pacific have weakened slightly (Figure 8(a)), as have the westerly wind anomalies near the dateline (Figure 8(c and d)). The cloud anomalies near the dateline have decreased slightly in magnitude, compared with the preceding period, but now extend to the Americas (Figure 8(b)). Turning to the Indian Ocean signal, larger areas of cool conditions are present in the southern midlatitudes during JFM of the El Niño composite, than in the preceding OND period (Figure 6(a) and Figure 8(a)). Elsewhere in the Indian Ocean, warm SST anomalies are evident, with slightly greater intensity than in the preceding period. Most of the central and eastern tropical/subtropical Indian Ocean show negative wind and cloud anomalies (Figure 8(b–d)), which would tend to warm local SST. Stronger winds (Figure 8(c and d)) are seen over most of the southern midlatitudes which, together with areas of increased cloud anomalies (Figure 8(b)), are consistent with cool SST anomalies there.

As the El Niño signal in the Pacific Ocean begins to attenuate during the AMJ period, the MSLP dipole across the entire domain dissipates (Figure 7(b)), and warm conditions over the Indian Ocean north of the southern midlatitudes weaken slightly (Figure 9(a)). Smaller areas of weaker winds (Figure 9(c and d)) and reduced cloud (Figure 9(b)) are now evident in the central and eastern tropical/subtropical Indian Ocean and winds have significantly strengthened (Figure 9(c)) east of Madagascar. Most of the north Indian Ocean shows weak wind anomalies and reduced cloud (Figure 9(b–d)) consistent with the SST anomalies there, being similar in magnitude to, or perhaps even larger, than those in the previous period (Figure 8(a)).

Conditions during the following JAS period show a complete change in MSLP anomalies towards a mixed pattern across the domain (Figure 7(c)). Positive anomalies in SST occur over the north Indian Ocean, and negative anomalies over the southern midlatitudes, whereas the warm signal in the tropical south Indian Ocean has further weakened (not shown). At the same time, cool anomalies have begun to appear in the eastern equatorial Pacific (not shown), westerly wind anomalies are no longer present (not shown), and the thermocline returns towards non-El Niño conditions (e.g. Philander, 1990). The areas of weaker winds and reduced cloud in the north Indian Ocean that may be associated with the warm SST anomalies there have contracted slightly compared to the previous period (Figure 9(b–d)). Most of the central south Indian Ocean, where the largest warm SST anomalies are located, shows weaker winds (not shown), as well as some areas of reduced cloud (not shown). There are stronger winds throughout most of the southern midlatitudes (not shown), consistent with the cool SST anomalies there (not shown).

By OND, there are negative MSLP anomalies over the northern Australian/Indonesian region, and positive MSLP anomalies over the south Pacific (Figure 7(d)). The area of cool SST anomalies in the southern midlatitudes of the Indian Ocean has expanded into large areas of the tropics of that ocean basin (not shown), as cool conditions have become established in the central and eastern tropical Pacific Ocean, along with a return to near climatological strengths of the easterly winds there (not shown). Stronger

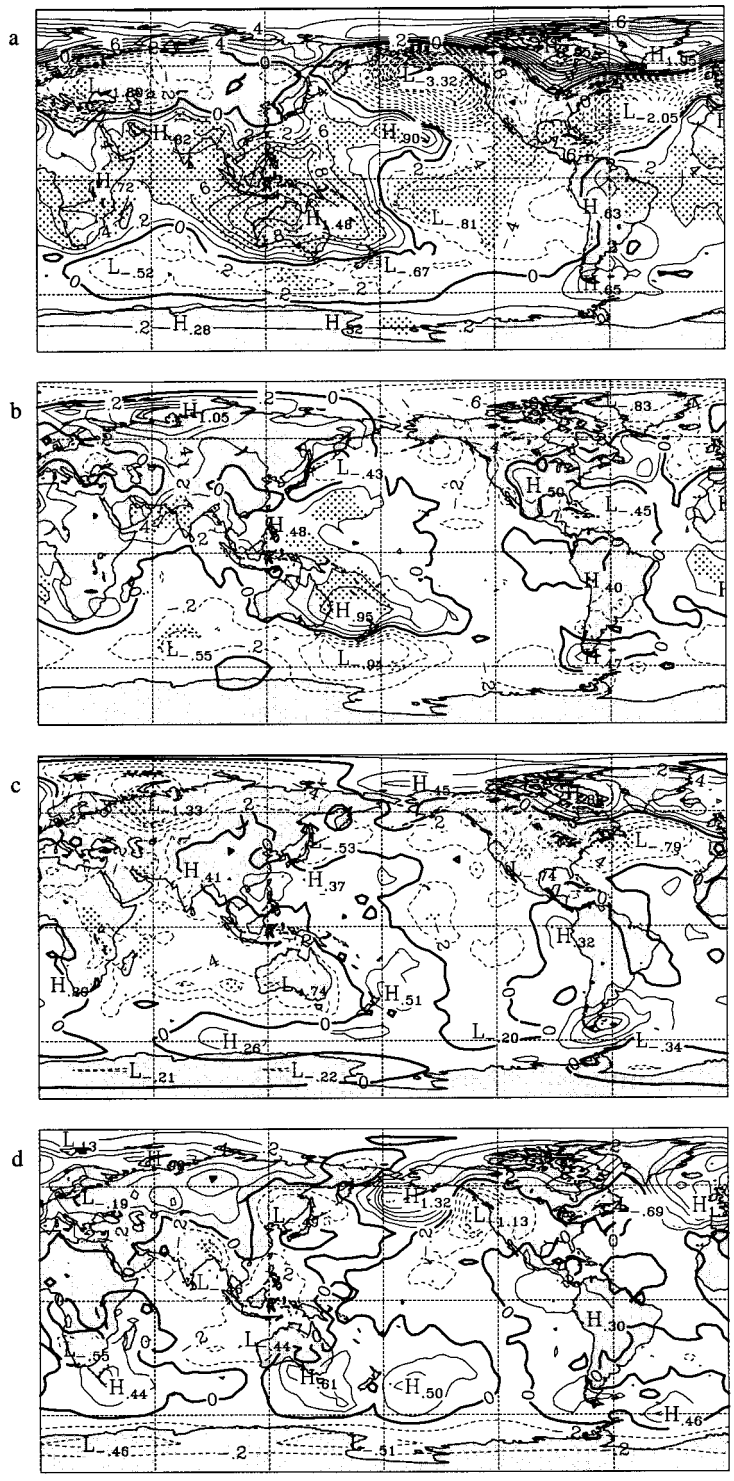

Figure 7. As in Figure 2, except showing El Niño composite sequence

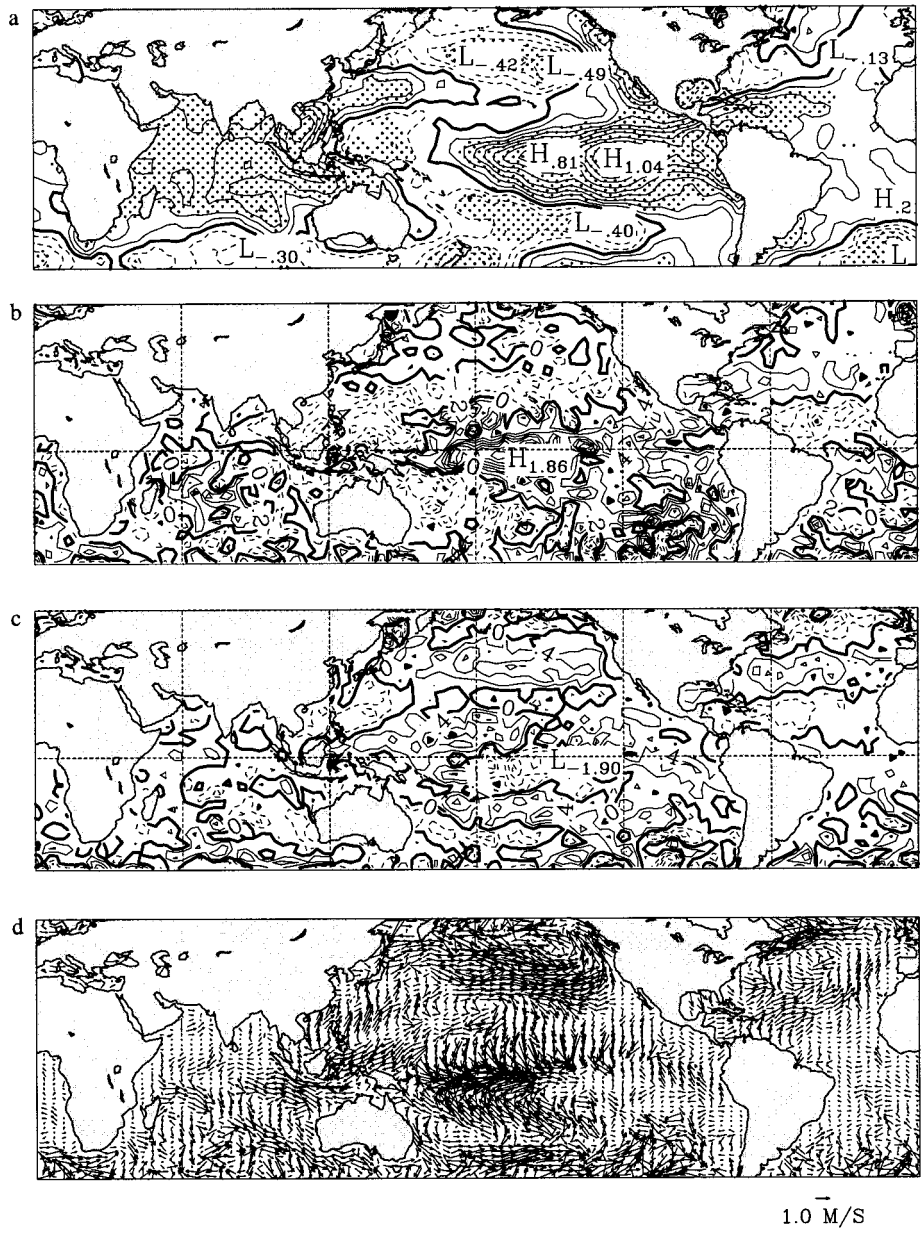

Figure 8. As in Figure 3, except showing El Niño composite sequence

winds (not shown) now exist over most of the Indian Ocean, except the southeastern region, and may be associated with this expansion of the cool SST anomalies northwards, and the weakening of the previous warm anomalies over the tropical Indian Ocean. Large areas of increased cloud (not shown) are also evident over much of the Indian Ocean, again favourable for weakening of the previously warm SST anomalies.

Thus, during the El Niño composite year, the Indo-Pacific MSLP dipole deteriorates, and the pattern of warm SST anomalies, except in the southern midlatitudes, slowly weakens throughout the year, so that the meridional gradient in SST anomaly in the subtropical south Indian Ocean significantly reduces. As with the El Niño-1 composites, it appears that the evolution in SST anomalies are broadly consistent with

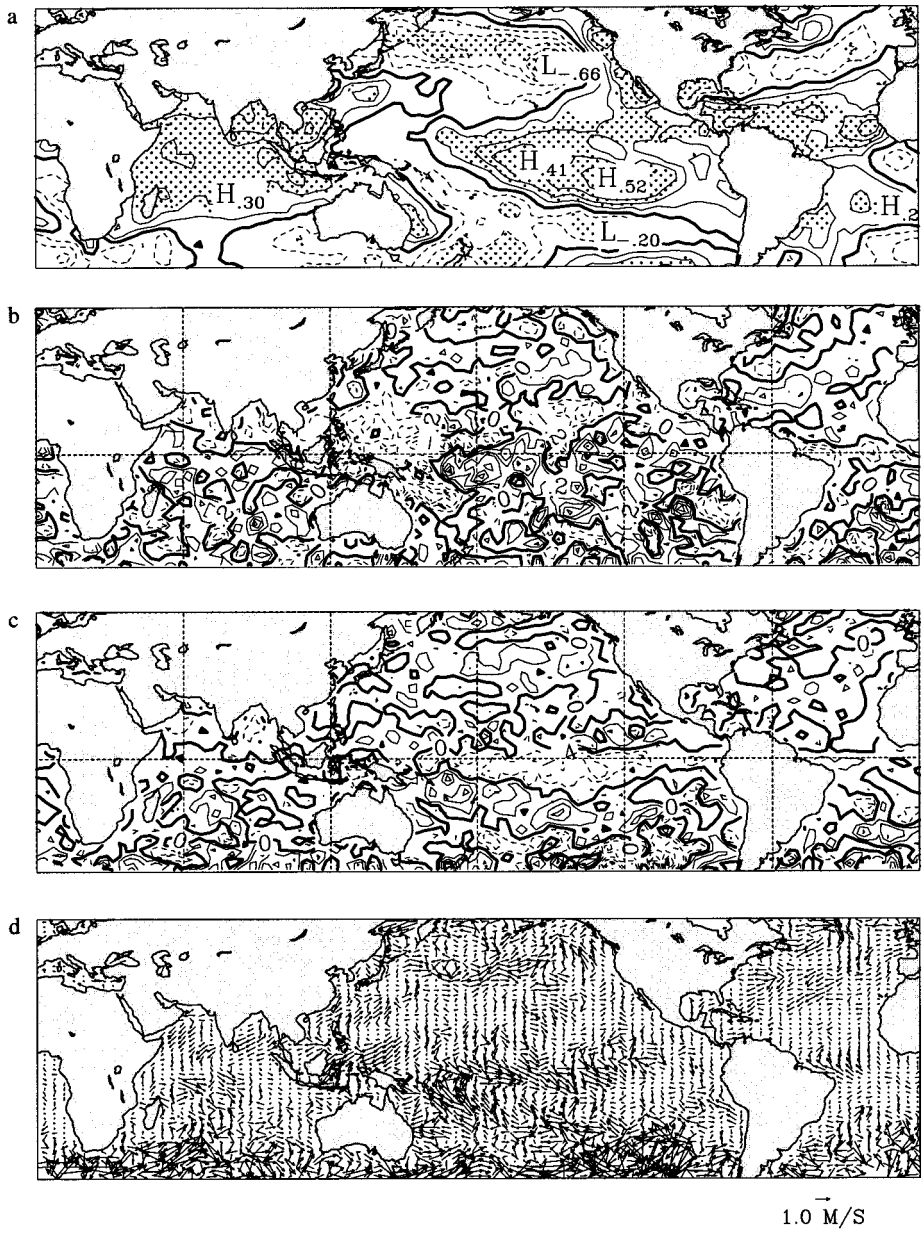

Figure 9. As in Figure 8, except for AMJ season

regions of anomalously weaker winds and reduced cloud for positive SST anomalies, and stronger winds and cloudier conditions where SST is cooler. This evolutionary pattern, therefore, suggests that the SST sequence mainly responds to changes in surface latent and sensible heat fluxes, and upper ocean mixing driven by the atmospheric changes. The JFM and AMJ periods immediately following the El Niño-1 composite also shows increased cloud cover east and north of Madagascar, which may reflect a shift in the ascending branch of a south Indian Ocean Walker circulation, as was suggested for the El Niño-1 composite.

3.3. La Niña-1

At the beginning of the sequence in the JFM season, MSLP anomalies show a rather mixed picture across the domain (Figure 10(a)). Most of the tropical Indian-Pacific to about 150°W displays warm SST anomalies, while conditions in the eastern Pacific are cool (warm) south (north) of the equator (Figure 11(a)). With the exception of the region south and southeast of Madagascar, and that immediately south of Australia, warm conditions prevail throughout the Indian Ocean (Figure 11(a)). Wind anomalies are relatively small throughout the tropical Pacific, except in the central equatorial region (Figure 11(c and d)), and represent stronger trade winds. Large areas of increased cloud are evident in the central and eastern equatorial Pacific Ocean, with negative anomalies in the western tropical Pacific Ocean (Figure 11(b)). In the Indian Ocean, wind anomalies are small, but negative over large areas (Figure 11(c and d)). Cloud cover is slightly increased over most of the north Indian Ocean, except off the Somali Coast, and decreased over large south Indian Ocean areas (Figure 11(b)). The north Indian Ocean SST anomalies are weakly positive (Figure 11(a)), and partially correspond to the areas of weaker winds. Both the SST warming, and the areas of weaker wind anomalies are, somewhat more intensified in large parts of the central to southeastern south Indian Ocean (Figure 11(a–d)). Large areas of decreased cloud are also evident (Figure 11(b)) which, with the weaker wind anomalies, would be favourable for warming of SST via changes to insolation and surface latent and sensible heat fluxes. The cool regions south of Australia, and in the southwest Indian Ocean, correspond to some extent with areas of increased winds and cloud cover (Figure 11(a–d)).

By the AMJ period, negative MSLP anomalies over the Indian Ocean to Australian regions, and positive MSLP anomalies across the Pacific Ocean, have begun to show the structure indicative of the La Niña phase of ENSO (Figure 10(b)). A pronounced cool anomaly is evident across the tropical Pacific, almost as far as the Philippines and Papua New Guinea (Figure 12(a)), with stronger trades throughout much of the western and central tropical Pacific (Figure 12(c and d)). The maritime continent region, and parts of the tropical to subtropical south Indian Ocean, have remained warm, while most of the north Indian Ocean now displays cool anomalies, as does the southwest Indian Ocean, and subtropical to midlatitude waters near Western Australia (Figure 12(a)). Wind anomalies in the Indian Ocean tend to be negative (Figure 12(c and d)) near regions of warmer SST, and *vice versa*, suggesting that wind driven changes to surface fluxes and upper ocean mixing may be contributing to the SST changes. The cloud signal is less clear but regions of increased cloud (Figure 12(b)) tend to correspond to cool SST, and *vice versa*, indicating that the SST signal in the Indian Ocean may also respond to changes in insulation.

During JAS, the Indo-Pacific dipole in the MSLP anomaly fields (Figure 10(c)) strengthens in the La Niña configuration. This is a time of intensified cool conditions in the central and equatorial Pacific, and enhanced trade winds in the central and western equatorial Pacific (Figure 13(a–d)), while almost all the tropical Indian Ocean west of 90°E is cool (Figure 13(a)). The Bay of Bengal region, Indonesian Seas, and their extension along the Western Australian Coast remain warm. The other area of warm Indian Ocean SST is in the region of the Agulhas Current system and its outflow across the southern midlatitudes (Figure 13(a)). The warmer Indonesian seas region experiences easterly anomalies in the western equatorial Pacific, and anomalous northwesterlies in the eastern equatorial Indian Ocean, together with reduced wind magnitudes (Figure 13(c and d)). Elsewhere in the Indian Ocean, winds are generally stronger in the central and western tropical to subtropical Indian Ocean (Figure 13(c and d)), and cloud cover increased (Figure 13(b)), consistent with the cooler SST over most of this region.

At the end of the composite year, OND, the east–west dipole in MSLP, reflecting a positive SOI phase, is strong and well-established (Figure 10(d)). The cool SST signal in the tropical Pacific is approaching its maximum, in conjunction with the region of enhanced easterly wind anomalies (Figure 14(a–d)), while the remaining warm region in the Indonesian Seas region has contracted, so that the entire north Indian Ocean is cool (Figure 14(a)). Only the waters near Western Australia and the southwest Indian Ocean are still showing warm anomalies. Almost the entire north Indian Ocean shows stronger winds (Figure 14(c)), consistent with cooler SST, and there are regions of increased cloud east of India (Figure 14(b)). The warm tongue of SST extending northwest from Australia seems to correspond to weaker easterly trades

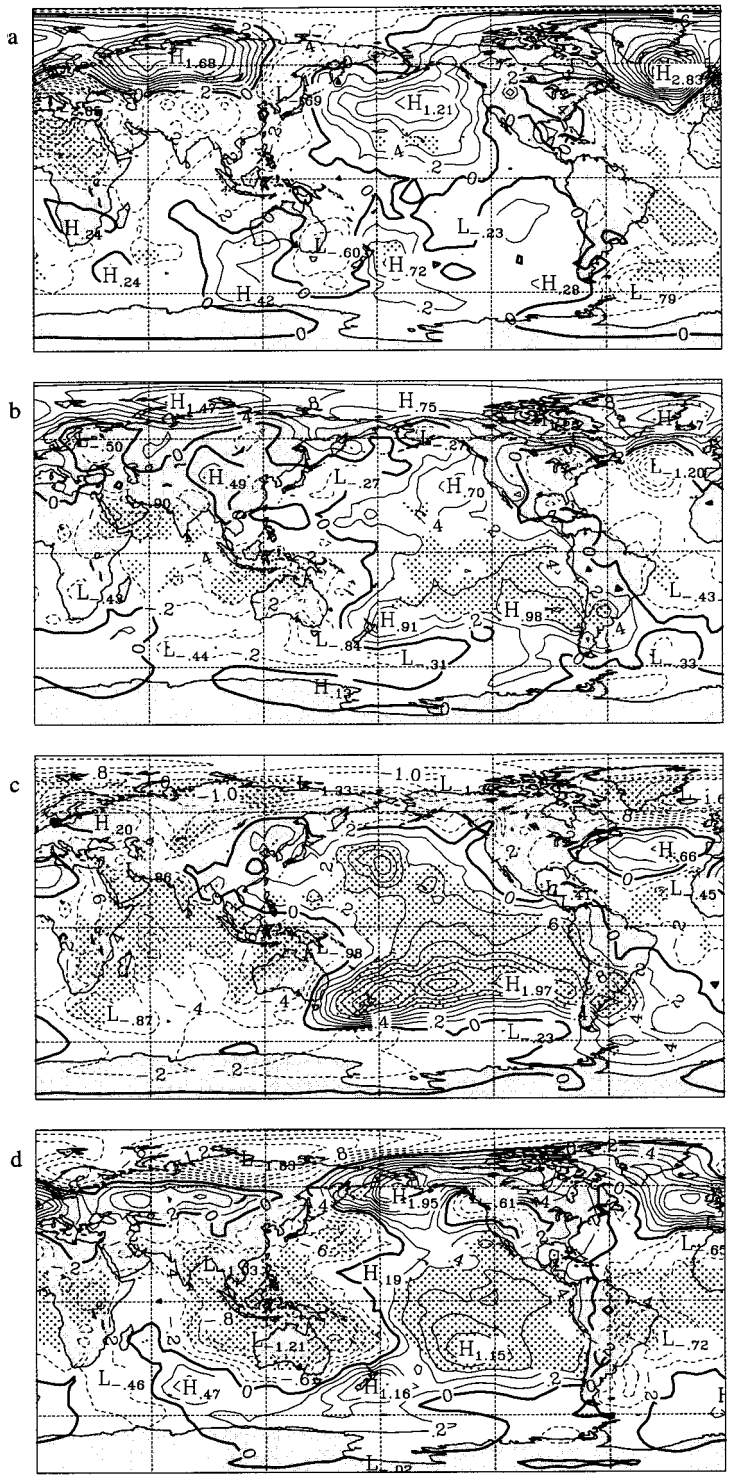

Figure 10. As in Figure 7, except showing La Niña-1 composite sequence

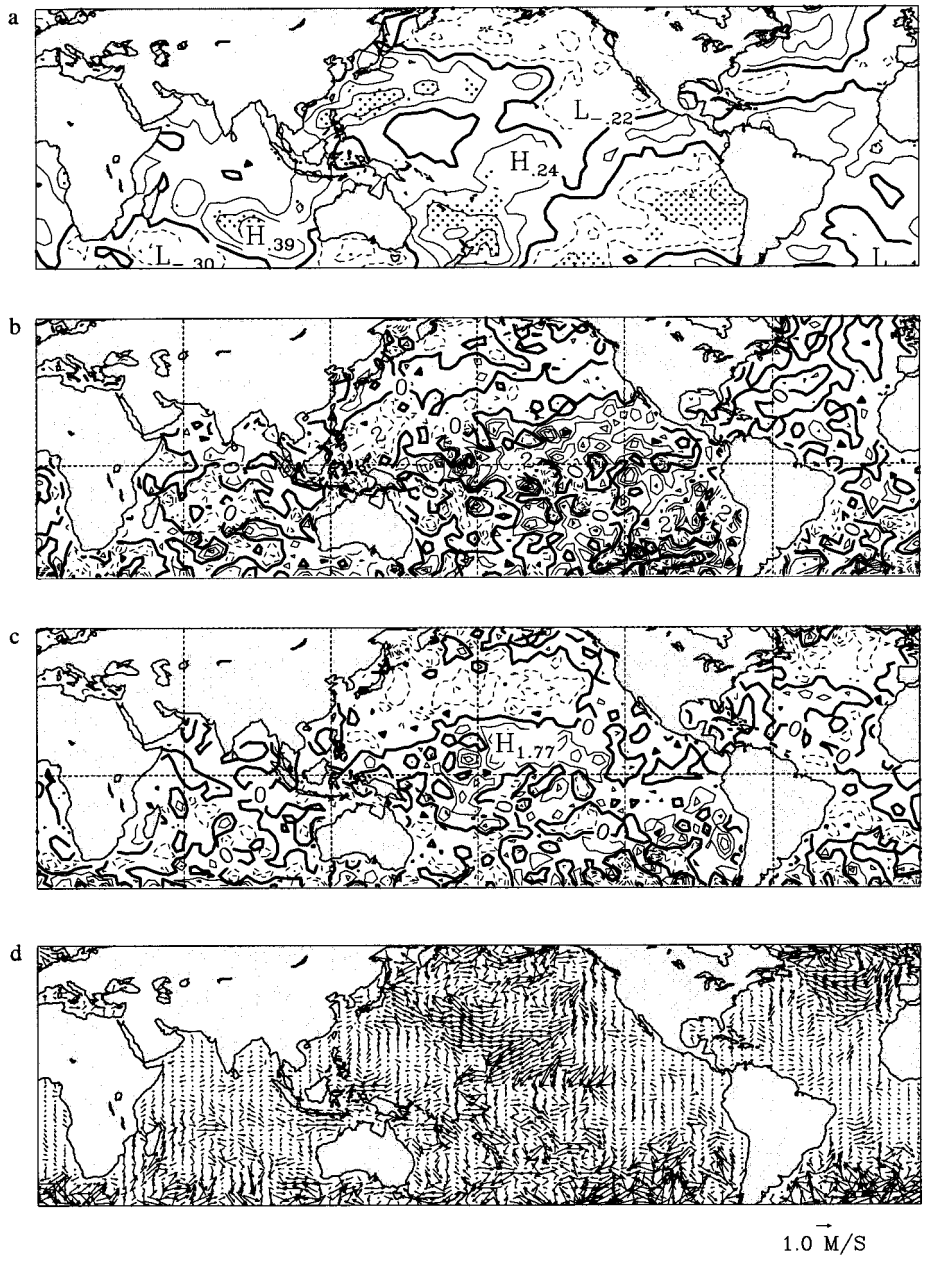

Figure 11. As in Figure 8, except showing La Niña-1 composite sequence

and to increased cloud cover (Figure 14(c and d)) linked to the commencement of the Australian monsoon season. In the central south Indian Ocean, there are large areas of stronger winds overlying the cool SST (Figure 14(a–d)), as well as regions of increased cloud here (Figure 14(b)). The warm SST in the midlatitude south Indian Ocean corresponds to some extent with weaker winds (Figure 14(a–d)) and reduced cloud (Figure 14(b)).

In summary, the La Niña-1 composite shows the development of the strong MSLP dipole across the Indo-Pacific domain, indicative of a positive phase in the SOI. The SST anomaly sequence indicates that an initially largely warm Indian Ocean evolves throughout the year to be mainly cool by the end of the year, except in the central southern midlatitudes, and northwest of Australia. The waters west and south

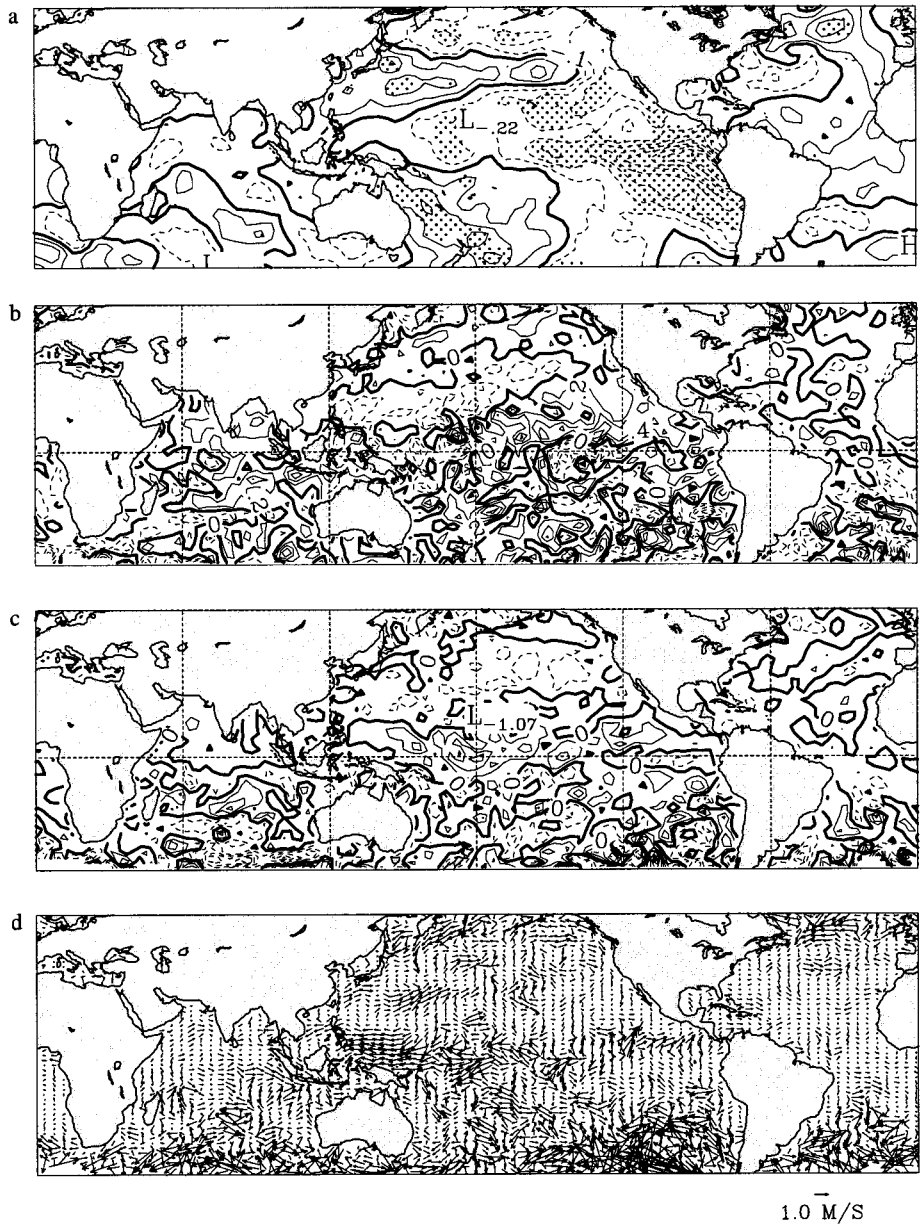

Figure 12. As in Figure 11, except for AMJ season

of Sumatra are, like the El Niño-1 signal, slowest to display the signal. Although there is some variation in the correspondence of the patterns, the essential feature appears to be one of cool SST regions corresponding to stronger winds and increased cloud and *vice versa*. This feature suggests that the SST is responding to the atmospheric changes via modulations of the surface latent, and sensible heat fluxes and upper ocean mixing. At least the OND period of the composite shows reduced cloud north, and immediately east, of Madagascar (the opposite of the El Niño-1), which may reflect a shift of the ascending branch of the tropical south Indian Ocean Walker circulation to lie over southern Africa (consistent with the lower pressure there), and less convection than usual over the southwest Indian Ocean.

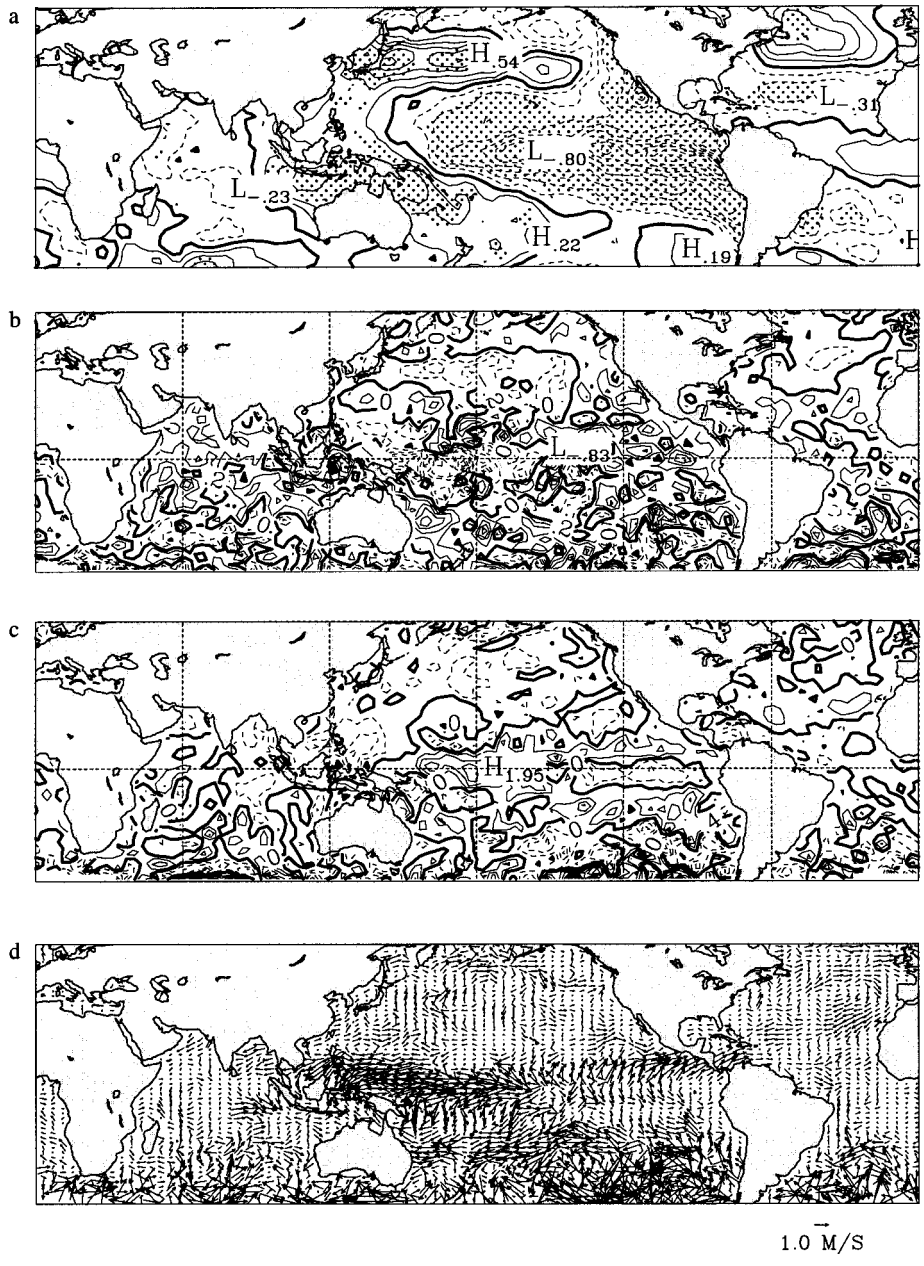

Figure 13. As in Figure 11, except for JAS season

3.4. La Niña

At the beginning of the composite year, JFM, the MSLP dipole dominates the domain, and is at its maximum intensity (Figure 15(a)). Cool conditions in the tropical Pacific have weakened slightly from the preceding period, as have the enhanced easterlies near the dateline (Figure 16(a–d)). Meanwhile, almost the entire tropical Indian Ocean shows cool anomalies, with warm conditions in the subtropical to midlatitude south Indian Ocean (Figure 16(a)). Winds are stronger over most of the north Indian Ocean and large areas of the tropical south Indian Ocean (except near Madagascar; Figure 16(c and d)), a pattern consistent with the cooler SSTs over much of the basin. Further south, in the Indian Ocean, most

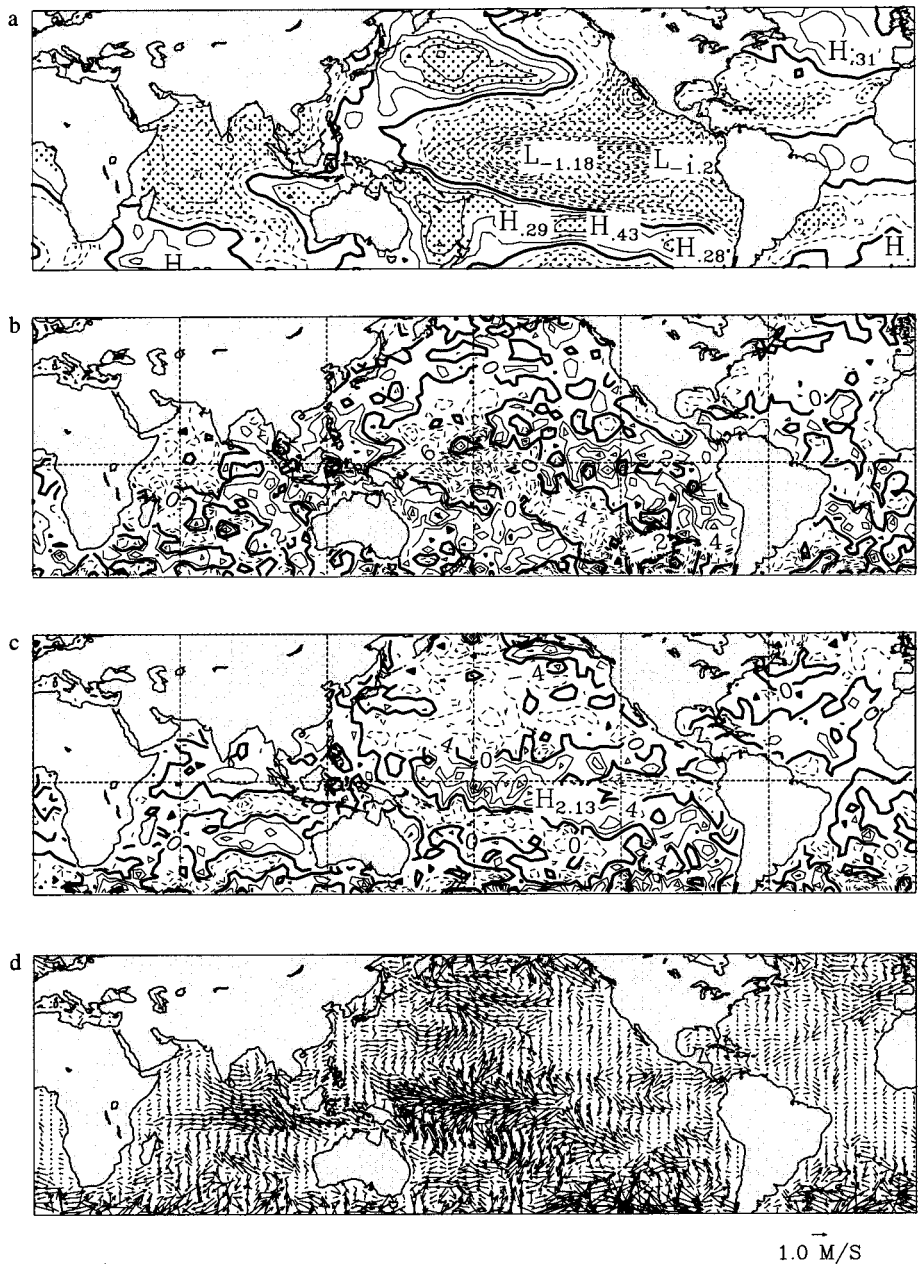

Figure 14. As in Figure 11, except for OND season

of the subtropical to midlatitude south Indian Ocean shows weaker winds (Figure 16(c and d)) that suggest thermodynamic links with the warmer SSTs at these latitudes (Figure 16(a)). The cloud patterns are more complex, but favour increased cloud over much of the north Indian Ocean (except near the Indian and Pakistani coasts), and eastern to central longitudes of the tropical south Indian Ocean (Figure 16(b)), once again consistent with cool SST anomalies there (Figure 16(a)). The southwest Indian Ocean shows a less obvious relationship between cloud and SST, although there are some regions of decreased cloud near regions of warm SST, and *vice versa* (Figure 16(a and b)).

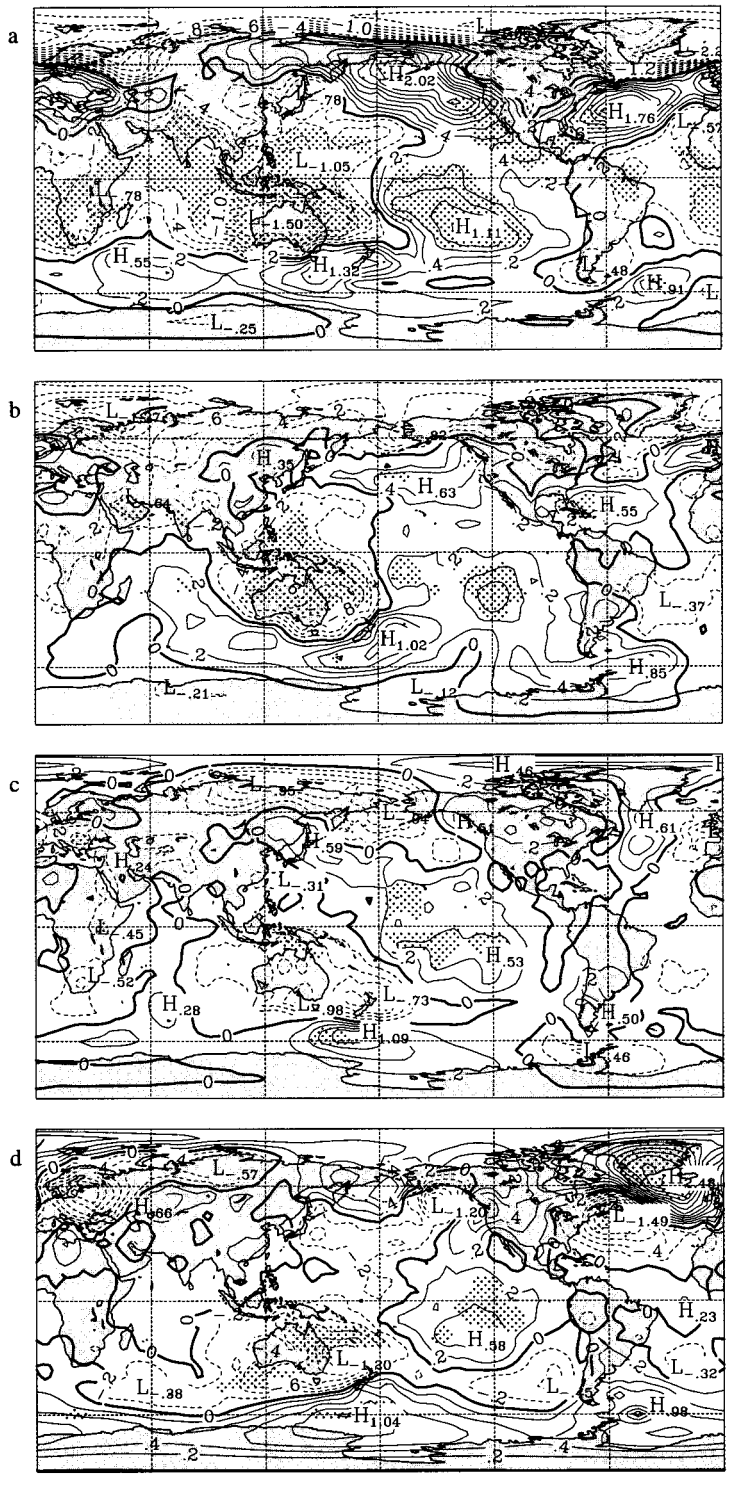

Figure 15. As in Figure 10, except showing La Niña composite sequence

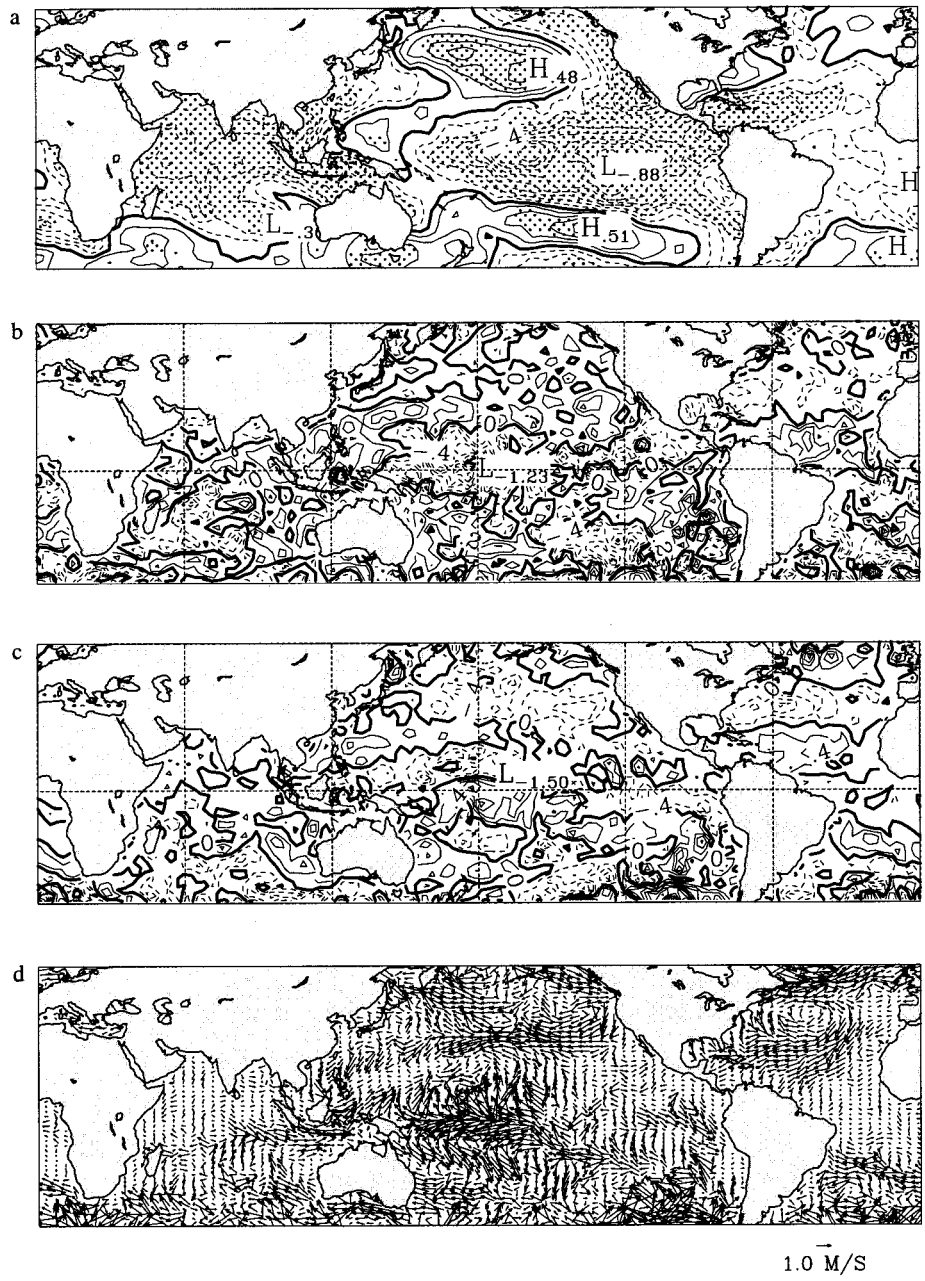

Figure 16. As in Figure 11, except showing La Niña composite sequence

For the following AMJ period, the MSLP dipole begins to collapse across the Indo-Pacific region, with weakening positive MSLP anomalies in the Pacific, and reduced negative MSLP anomalies over Australasia (Figure 15(b)). Cool conditions have intensified slightly in the tropical Indian Ocean, and also extend further south into parts of the midlatitude south Indian Ocean (Figure 17(a)), as the La Niña signal in the Pacific has weakened further (particularly as far as the wind anomalies are concerned), and lost some coherency in pattern (Figure 17(c and d)). Strong wind anomalies now exist throughout almost the entire north Indian Ocean and large parts of the tropical south Indian Ocean (Figure 17(c and d)), as expected if the SST changes are being driven by the wind. However, there is a sizeable region north and

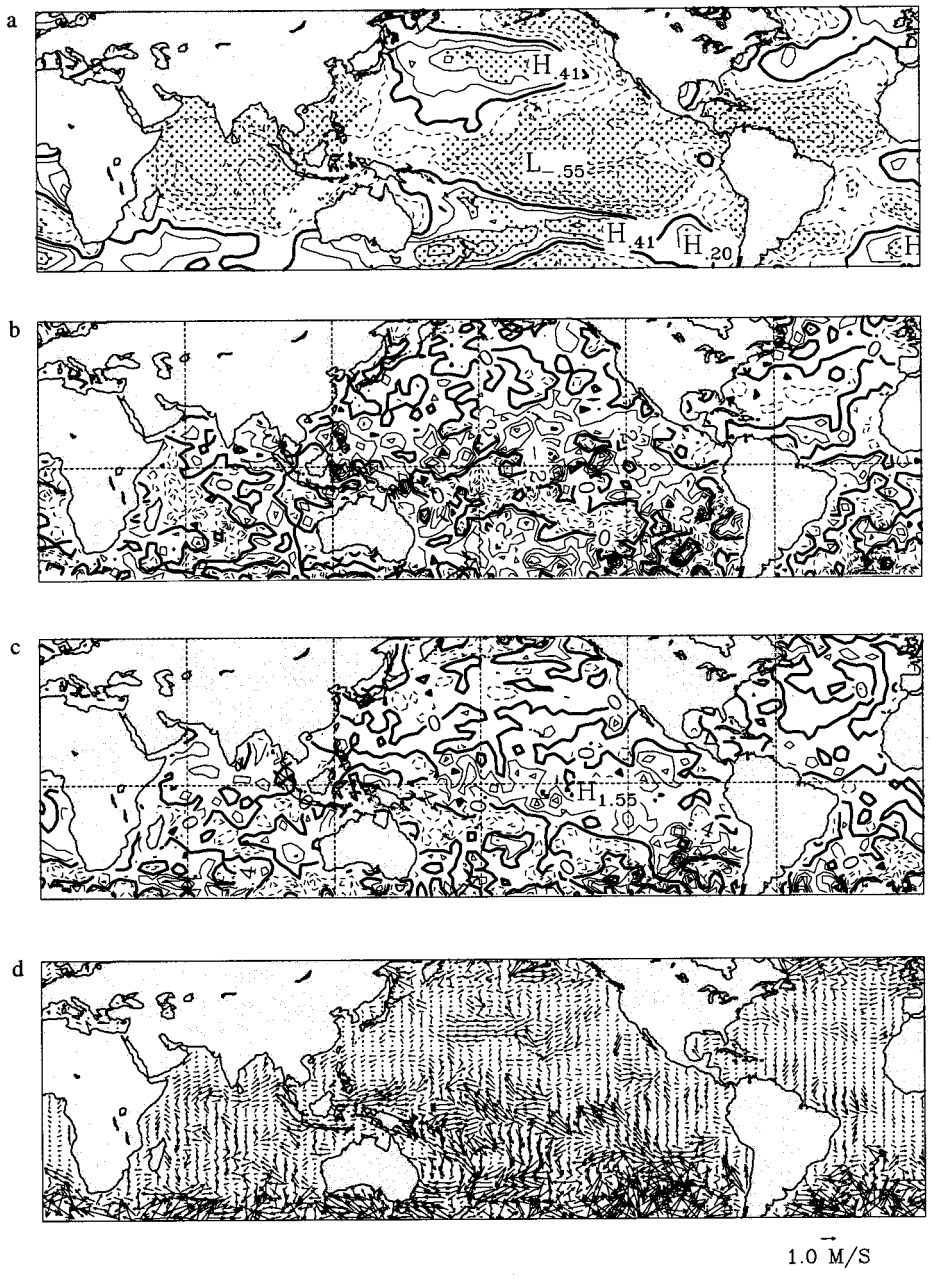

Figure 17. As in Figure 16, except for AMJ season

east of Madagascar, which shows both weaker winds and reduced cloud cover (Figure 17(b–d)), which might suggest warmer SST if the SST is only responding to the atmospheric forcing via local thermodynamic effects. The wind anomalies (Figure 17(c and d)) off the Tanzanian and east Madagascar coasts represent a weakening of the climatological southeasterly trades, and perhaps may reflect a decrease in convergence of warm surface waters near the coast, leading to relative cooling of SST there. Further south, the region of warm midlatitude SST anomalies corresponds to some extent to areas of weaker winds and reduced cloud (Figure 17(b–d)).

During JAS, the MSLP dipole weakens further, particularly over Australia and the Indian Ocean (Figure 15(c)). The cool SST anomalies in the tropical Pacific have weakened further, and some warm anomalies have appeared off the coast of Peru (not shown), as the wind anomalies are significantly reduced in magnitude (not shown). Similarly, the cool SST anomalies in the tropical Indian Ocean have been attenuated, as have the warm midlatitude anomalies in the south Indian Ocean (not shown). This situation is reflected by the appearance of some regions of weaker winds (not shown) in the tropical Indian Ocean, although cloud anomalies are mainly positive (not shown). Most of the southern midlatitudes of the Indian Ocean show weaker winds (not shown), consistent with warmer SST, but more mixed signals in cloud cover anomalies (not shown). In the eastern tropical south Indian Ocean, there is weakening of the southeasterly trades (not shown), which would be favourable for the warming observed in the Indonesian Seas region (not shown).

The final period, OND, still sees a weak MSLP dipole in a similar alignment to that observed in the previous JAS season (Figure 15(c and d)). It is, thus, not surprising that similar SST anomalies to the preceding period (not shown) occur in both the Indian and tropical Pacific Oceans, except that the warm Indonesian seas region has cooled, as has that near Peru. The wind magnitudes and directions (not shown) are also similar to the preceding JAS period in both the Indian and tropical Pacific Oceans, reflecting the weakening La Niña signal there. Large areas of reduced cloud anomaly (not shown) are now apparent in the tropical western Indian Ocean, favourable for weakening of the cool SST anomaly there (not shown). However, in the western half of the southern midlatitudes, stronger winds observed previously (not shown) are now largely reduced in magnitude (not shown), and appear to correspond to a warming in the region south of Africa.

In summary, it appears that the basic La Niña signal in Indian Ocean MSLP and SST anomalies remains throughout the composite year, although a noticeable weakening is evident. This weakening of the signal is broadly consistent with the evolution in the wind and cloud cover anomalies throughout the composite period, although the relationship of cool SST, where winds are stronger and cloud increased, and *vice versa*, is less obvious than during the preceding La Niña-1 composite year. Presumably, other processes, such as dynamical adjustment of the ocean circulation to the winds and, as suggested by Godfrey *et al.* (1995), tidal mixing in the Indonesian Seas may contribute, together with thermodynamic effects, to observed SST changes in the Indian Ocean. Most of the composite year shows reduced cloud cover near Madagascar, which is consistent with an intensified ascending branch of the Walker circulation over tropical southern Africa and reduced convection over the tropical southwest Indian Ocean during La Niña events (Tyson, 1986; Lindesay, 1988).

4. QB AND LF BAND SEASONAL COMPOSITES OF MSLP AND SST ANOMALIES

4.1. El Niño-1

The JFM season at the start of this sequence shows somewhat contradictory signals between QB and LF MSLP anomaly patterns, and mixed SST distributions (Figure 18(a–d). On the QB band, the MSLP distribution is more indicative of La Niña conditions, while the LF MSLP pattern is suggestive of an El Niño configuration (Figure 18(a and c)). As much of the raw MSLP signal is carried by the QB and LF bands, the tendency for opposite phases of ENSO to occur in these bands at this time may lead to a very mixed raw JFM MSLP composite signal in Figure 2(a). The SST patterns on the QB and LF bands are less distinct, although the QB exhibits something of a weak La Niña structure across the Pacific (Figure 18(b)). In the Indian Ocean, the QB band suggests a weak SST dipole structure, particularly over the eastern portion on the basin (Figure 18(b)).

For the second season, AMJ, both the QB and LF bands for MSLP show varying degrees of an El Niño signal (Figure 19(a and c)). However, the LF distribution is far more coherent and robust across the Indo-Pacific domain, and appears to carry the bulk of the developing El Niño pattern in the raw MSLP anomaly field (Figure 2(b)). For SST, both bands have varying degrees of the El Niño signal, but the LF

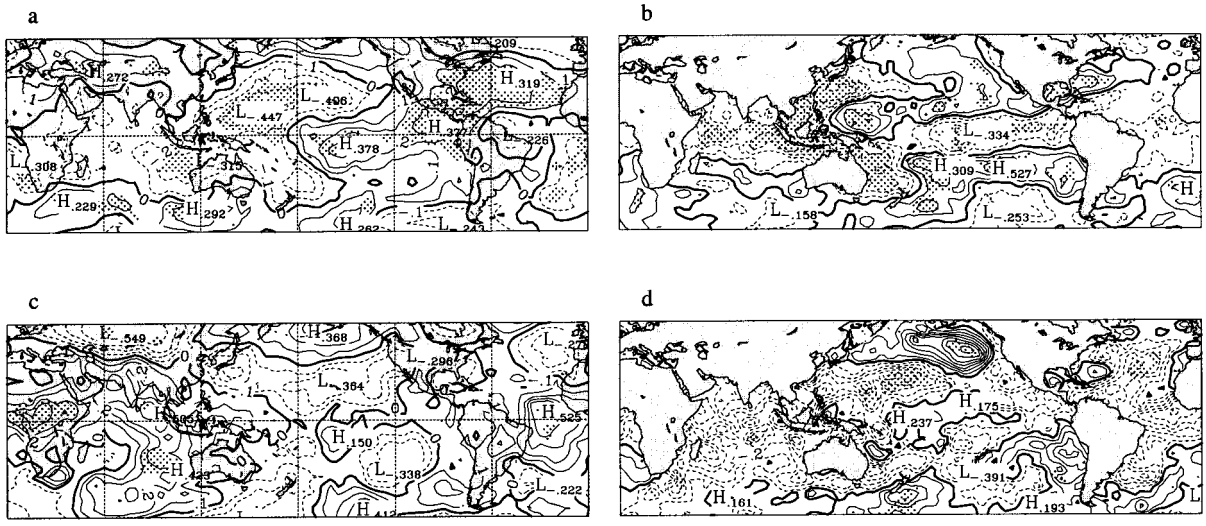

Figure 18. Band pass filtered JFM seasonal El Niño-1 composite sequences of (a) QB (2–2.5-year) band MSLP, (b) QB (2–2.5-year) band SST, (c) LF (2.5–7-year) band MSLP, and (d) LF (2.5–7-year) band SST anomaly fields over the period 1878–1994. Events used in the filtered composites are given in Table I. MSLP are in hPa (plotted every 0.1 hPa), and SST are in °C (plotted every 0.1°C). Dashed (solid) contours denote negative (positive) values. Significant *t*-test areas at the 95% level are stippled

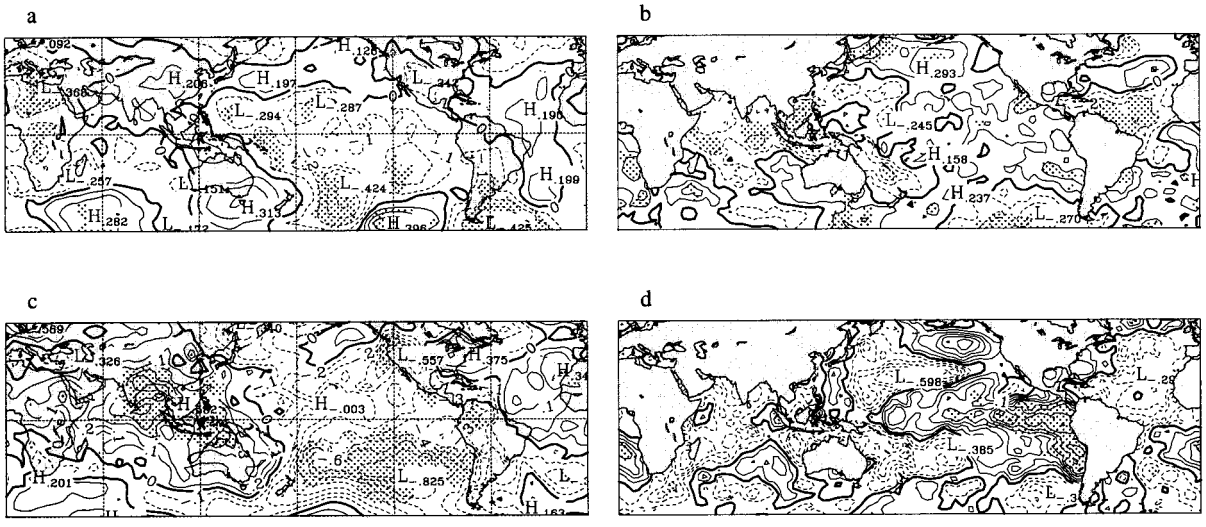

Figure 19. As in Figure 18, except for AMJ season

band has a far more coherent warm SST anomaly across the equatorial central–eastern Pacific (Figure 19(b and d)). Over the Indian Ocean, there is little evidence of the underlying dipole pattern in SST across the eastern portion of the basin in the raw composite (Figure 4(a)), but both QB and LF bands show distinct but somewhat contrary dipole patterns in that region (Figure 19(b and d)). Consequently, the superposition of the QB and LF signals leads to the loss of these patterns in the raw SST composite. This is an important finding during the AMJ season, as Australian studies indicate the tendency for such SST dipole patterns to develop around the austral autumn (boreal spring) season (Nicholls, 1989; Drosdowsky, 1993a,b; Smith, 1994; Allan *et al.*, 1996). These SST dipole stuctures have been linked with Australian rainfall variability. It would seem that a predominance of slightly different eastern Indian Ocean SST dipole patterns can emerge if either of the QB or LF bands is dominant over the other at this time of the year.

By JAS, the MSLP anomaly fields show that, although both bands have similar dipole patterns, the LF band is the major source of the El Niño signal in MSLP across the domain (Figure 20(a and c)). This can be clearly seen if the raw MSLP signal in Figure 2(c) is contrasted with Figure 20(a and c). A similar situation is evident with regard to SST anomalies, where the LF band has a pronounced warm SST signal across the tropical Pacific, with positive anomalies also in the far western and central Indian Ocean (Figure 20(b and d)), displaying a similar pattern to the raw SST signal though enhanced in magnitude (Figure 5(a)). Only a moderate to weak equatorial Pacific warming pattern is evident on the QB band, with weak SST structures in the Indian Ocean Basin including an eastern Indian Ocean dipole (Figure 20(b)). However, on the LF band, both the western and eastern portions of the Indian Ocean show evidence of distinct dipole structures, in a pattern containing the dipole of Chambers *et al.* (1999), Saji *et al.* (1999) and Webster *et al.* (1999). Interestingly, the studies noted above, in the previous season of the sequence, suggest that a number of eastern Indian Ocean dipole patterns can occur. As a result, such SST dipole structures can provide varying degrees of influence on the spatial alignments of atmospheric moisture feeding into parts of the Australian continent via tropical-temperate cloud band systems linked to prefrontal troughs ahead of midlatitude cold frontal passages.

By the end of the El Niño-1 sequence in OND, a strong El Niño signal is apparent, with the LF MSLP band again dominant (Figure 21(a and c)). At this time, the positive MSLP anomaly over Australasia is particularly coherent on the LF band, with a secondary centre over southern Africa and negative MSLP anomalies over much of the central–eastern Pacific and in the central south Indian Ocean. However, both bands can be seen to contribute elements to the overall raw MSLP pattern in Figure 2(d). With the SST anomaly fields, the LF band is again dominant, although the overall raw SST pattern (Figure 6(a)) is also shaped by contributions from the QB signal (Figure 21(b and d)). The eastern Indian Ocean dipole pattern is most evident in the filtered SST fields on the LF configuration (Figure 21(d)), and contains the mature stage of the dipole of Chambers *et al.* (1999), Saji *et al.* (1999) and Webster *et al.* (1999). As noted earlier, the raw SST pattern loses much of the distinct eastern Indian Ocean dipole if both the QB and LF signals are closely aligned, and in this case would be most defined under conditions where the LF band prevails over the QB band.

To summarize, the El Niño-1 sequence in the QB and LF bands shows that the evolution of an El Niño event in MSLP and SST anomaly fields is most strongly manifest on the LF band. However, as the event approaches significant proportions, the QB band makes increasingly important contributions to the overall patterns in both MSLP and SST anomaly fields. Over the Indian Ocean Basin, the evolving El Niño signal across the western–central parts of the basin can also be seen to embrace the changing nature

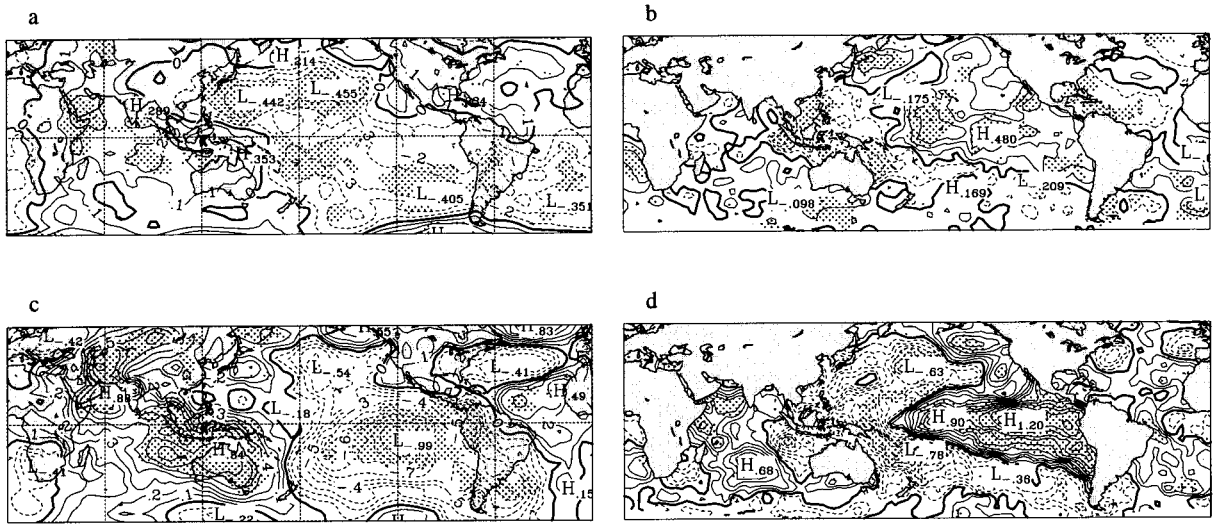

Figure 20. As in Figure 18, except for JAS season

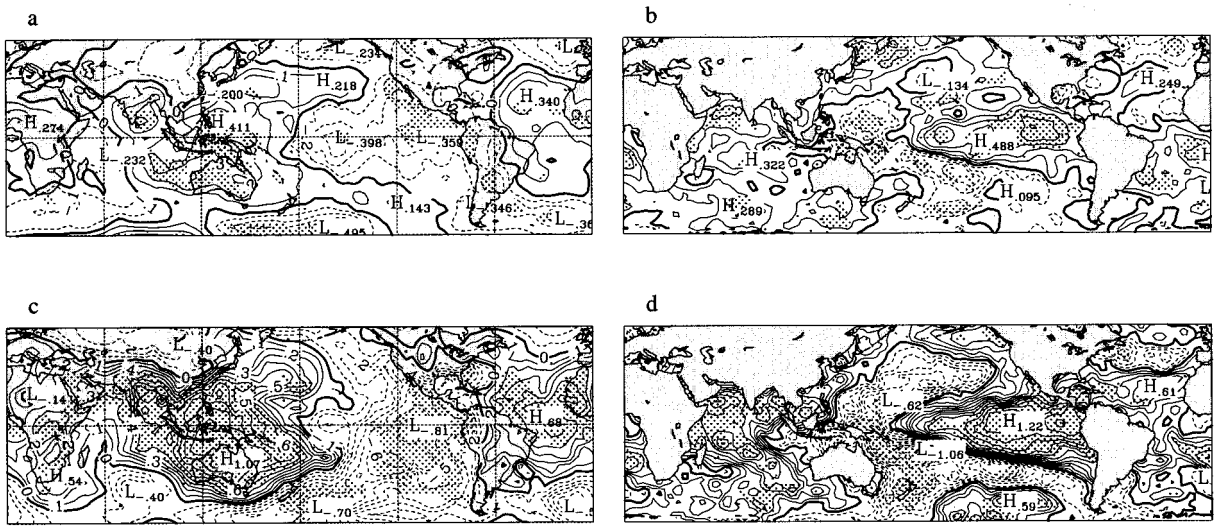

Figure 21. As in Figure 18, except for OND season

and structure of SST dipole patterns over the eastern portion of the region. Such dipoles are carried on both the QB and LF bands, but are often lost in the superposition of these signals into the raw SST composites. Thus, manifestations of such SST dipole patterns are most likely to be enhanced in particular El Niño events, when one of either the QB or LF signals is dominant over the other.

4.2. El Niño

The mature phase of an El Niño event across the Indo-Pacific domain tends to be reached by the JFM season. During this period, the LF band continues to carry the strongest MSLP signal, with there being important contributions from the QB band (Figure 22(a and c)). This nature is also reflected in the patterns of SST in both bands, with the structure inherent in the raw data (Figure 8(a)) dominated by the contribution from the LF distribution (Figure 22(b and d)). During this season there is no evidence of distinct SST dipole patterns across the Indian Ocean Basin, apart from the north–south gradient in SST

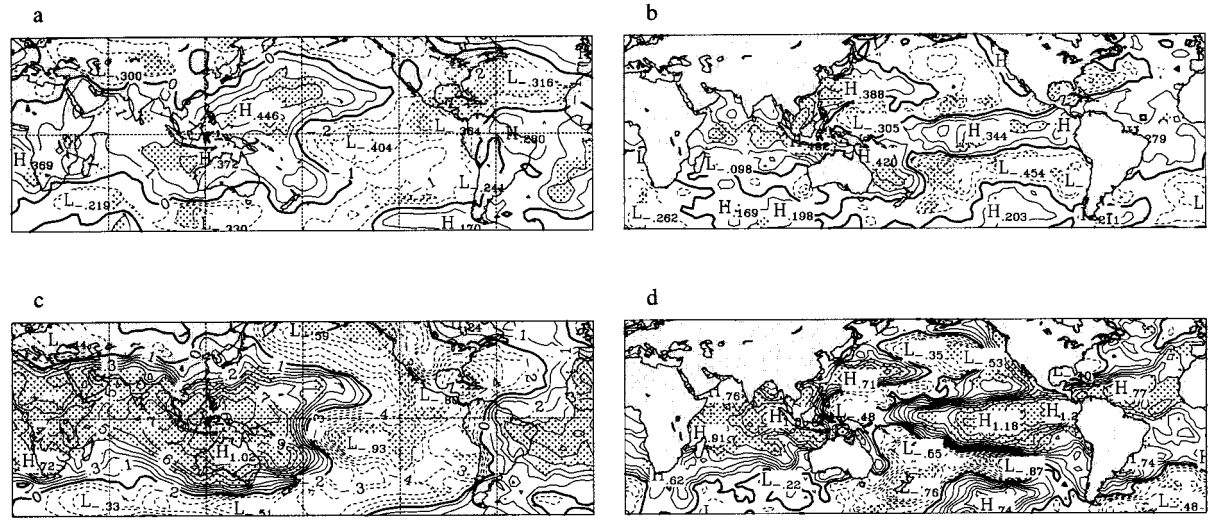

Figure 22. As in Figure 18, except showing El Niño composite sequence

typical of the El Niño response, where strong warming occurs over all but the southern midlatitudes of that ocean.

By AMJ, the El Niño event begins to show signs of waning, as the MSLP east–west dipole pattern across the Indo-Pacific region is strongly carried on the LF band (Figure 7(b) and Figure 23(a and c)). In fact, the QB band has already begun to show signs more in line with La Niña conditions than El Niño (Figure 23(a)). As a consequence of the disparity between the QB and LF MSLP signals, the Pacific node of the MSLP dipole, indicative of the Southern Oscillation, is much weaker in the raw MSLP field (Figure 7(b)). The SST fields confirm much of what is seen in the MSLP data in the QB and LF bands. The LF SST pattern (Figure 23(d)) is the only one to show anything of the El Niño signal in either ocean basin. Across the Indian Ocean, the QB band carries strong western and eastern Indian Ocean SST dipoles, which show little manifestation in the raw SST field in this season (Figure 9(a) and Figure 23(b)). This finding is again important for Australia, and possibly southern Africa (Lindesay, 1988; Walker, 1990; Mason, 1995; Rocha and Simmonds, 1997a,b; Reason, 1998), with the prospect of varying Indian Ocean SST controls on rainfall systems depending very much on the balance between QB and LF signals.

As the sequence shifts to the JAS period, the El Niño event has collapsed in the atmosphere. MSLP conditions in the QB band are now indicative of a weak La Niña episode, and the LF band MSLP anomalies are dominated by negative MSLP across most of the Indo-Pacific region (Figure 24(a and c)). With the SST fields, weak to moderate El Niño-like conditions are still evident in both the Indian and Pacific Ocean Basins in the LF band (Figure 24(d)). However, this is countered by something approaching a weak La Niña pattern in equatorial Pacific SSTs on the QB band (Figure 24(b)). Nevertheless, the raw SST anomalies (not shown) indicate that the LF signal is still dominant in most regions, with weakening El Niño conditions over the Indo-Pacific Basin. Both the QB and LF bands show a hint of western and eastern Indian Ocean SST dipole structures.

By the end of the sequence in OND, the QB band continues to favour weak–moderate La Niña conditions with an MSLP dipole across the Indo-Pacific domain carrying a positive SOI pattern (Figure 25(a)). On the other hand, the LF MSLP signal is very incoherent, and leads to the overall raw MSLP pattern being ill-defined (Figure 7(d) and Figure 25(c)). Not surprisingly, the SST distributions in the QB and LF band and the raw signal are mixed. Interestingly, the raw SST pattern shows a mixture of weak La Niña conditions in the Pacific, and weak El Niño in the Indian Ocean Basins (not shown). Relatively weak dipole patterns remain evident in the Indian Ocean on the LF band.

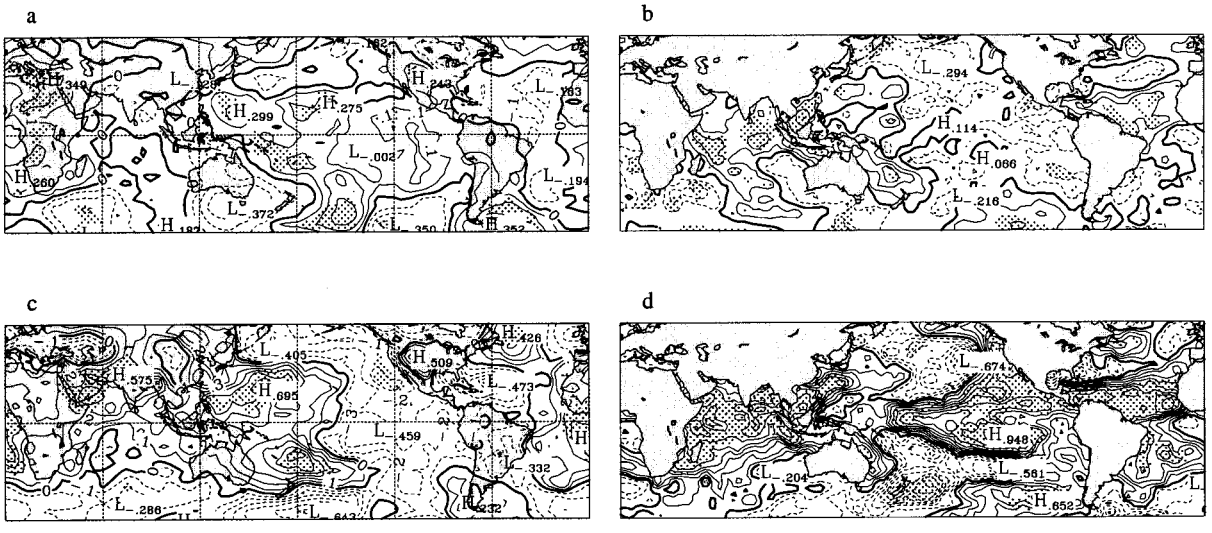

Figure 23. As in Figure 22, except for AMJ season

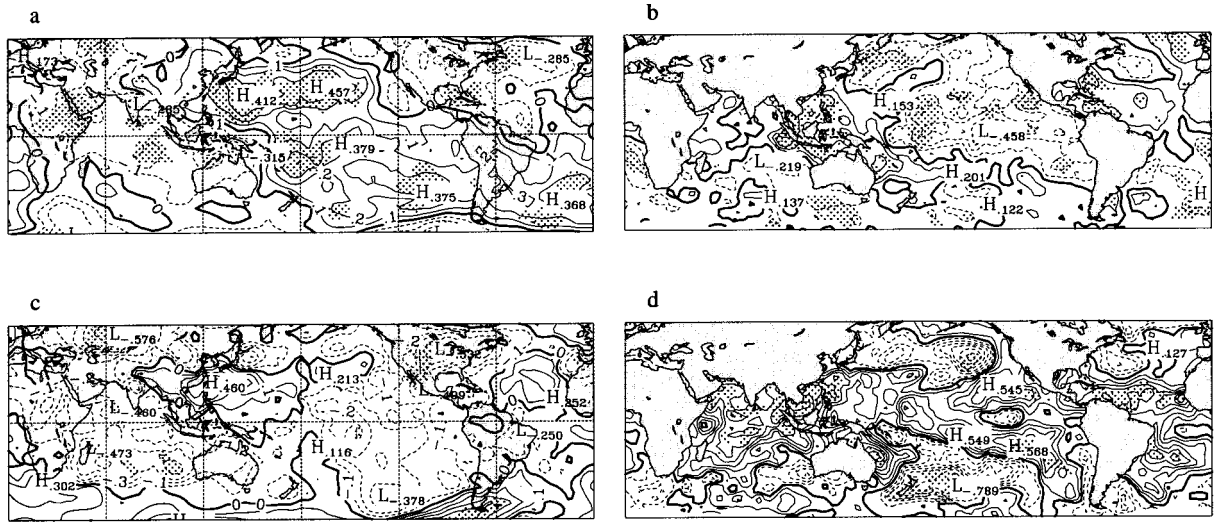

Figure 24. As in Figure 22, except for JAS season

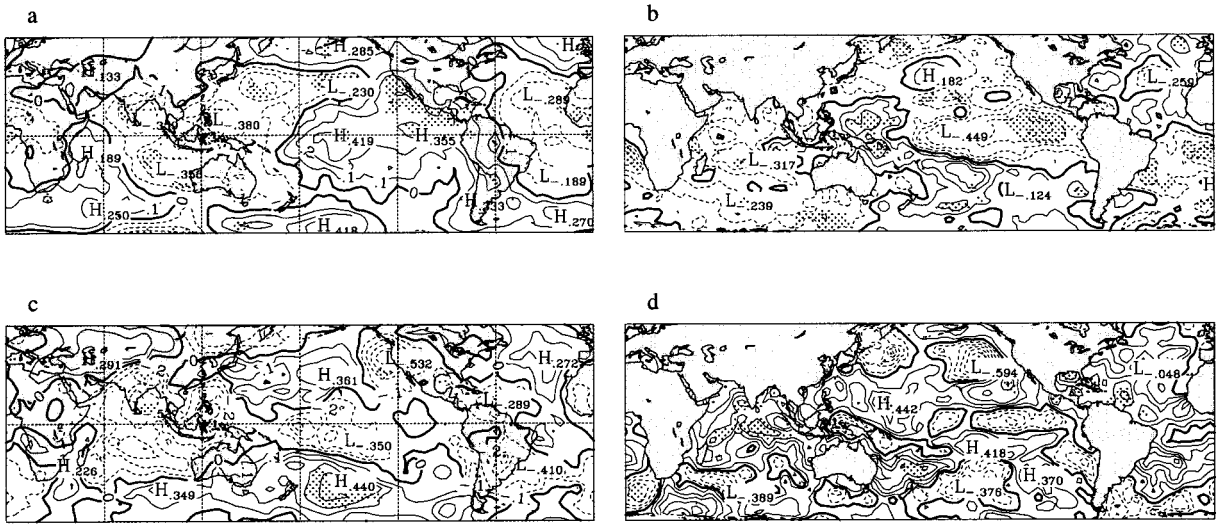

Figure 25. As in Figure 22, except for OND season

In summary, the demise of El Niño during this sequence is found to be most strongly manifest on the QB band, where there is a rapid switch to La Niña-like patterns in MSLP and SST anomalies after the JFM peak in the phenomenon. On the LF band, there is a quite definite tendency for El Niño conditions to persist throughout much of the sequence, particularly with regard to SSTs in the Indian Ocean region. As with the evolution into an El Niño, the austral autumn–winter (boreal spring–summer) shows a strong tendency to favour SST dipole patterns in the eastern portion of the Indian Ocean on the QB band. Such structures are overwhelmed when the LF band is strong, but would be very prominent in circumstances when the QB signal is dominant.

4.3. La Niña-1

In the JFM period beginning this sequence, the MSLP patterns in the QB and LF band and the raw data show a fairly disorganized response across the Indo-Pacific region that favour neither El Niño or La

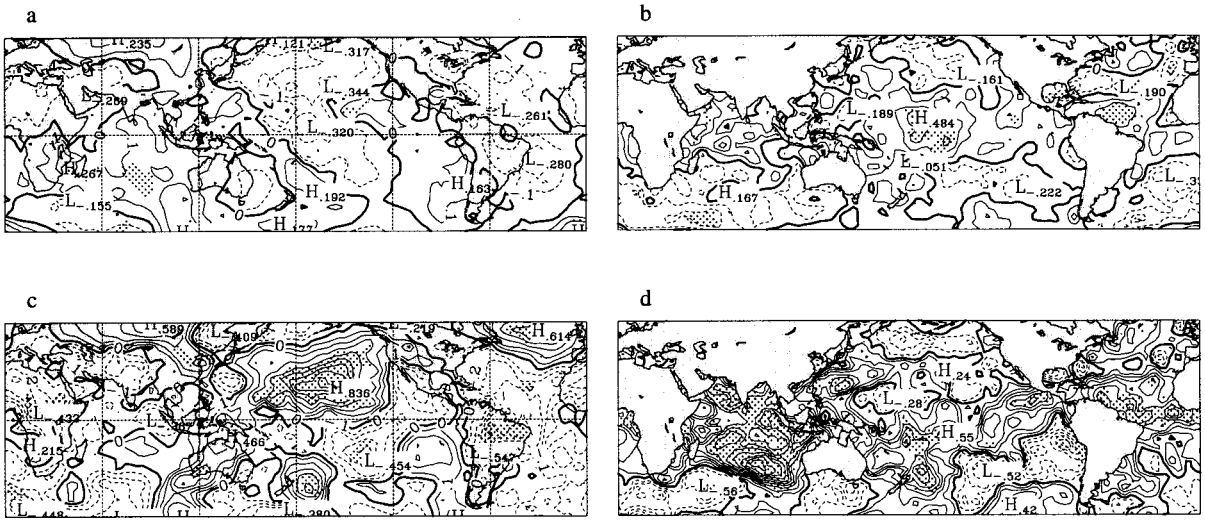

Figure 26. As in Figure 18, except showing La Niña-1 composite sequence

Niña conditions (Figure 10(a) and Figure 26(a and c)). The SST anomaly fields in both the QB and LF bands are indicative of a weak warm event across the tropical Indo-Pacific Basin (Figure 26(b and d)). Over the Indian Ocean, there is a suggestion of a SST dipole pattern on both western and eastern margins of the basin in the QB band. Not surprisingly, the poor structural nature of the SST data in the Pacific on the QB and LF bands is reflected in the raw SST pattern, while in the Indian Ocean the LF band appears to dominate (Figure 11(a)).

By AMJ, the LF band begins to show evidence of a developing La Niña event in MSLP, with the formation of a dipole pattern across the Indo-Pacific domain that is indicative of the positive phase of the Southern Oscillation (Figure 27(c)). The QB band has something of the positive MSLP node of the dipole in the Pacific, but is mixed in its MSLP pattern over the western Pacific and Indian oceans (Figure 27(a)). As expected, the SST anomalies show most signs of an evolving La Niña through the cool SSTs along the western–eastern equatorial Pacific on the LF band (Figure 27(d)). On the QB band, the SST signal is still quite disorganized, although there is a strong suggestion of the development of a cold SST 'tongue' in the

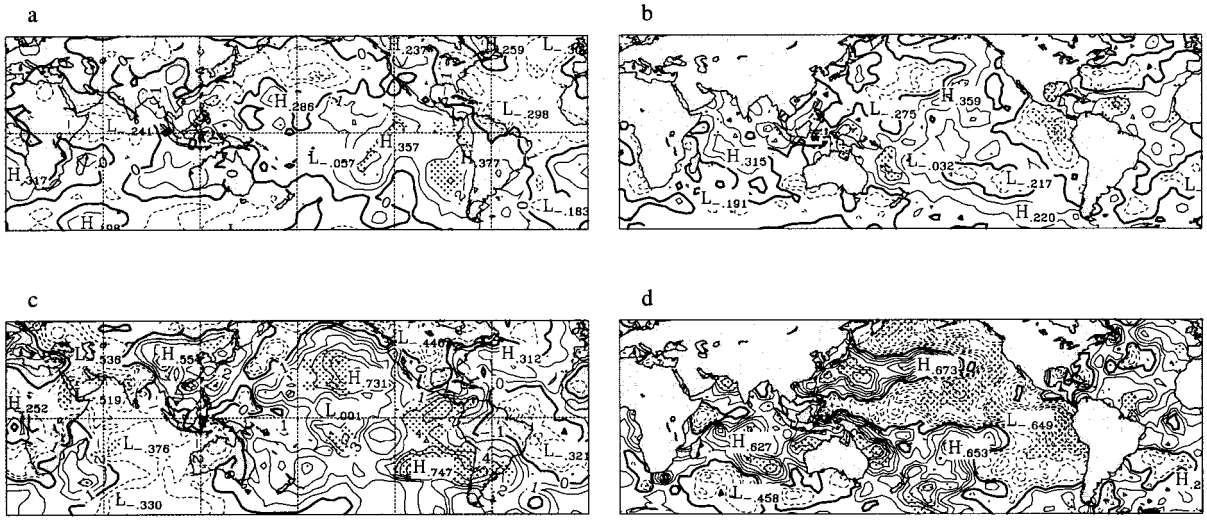

Figure 27. As in Figure 26, except for AMJ season

far eastern equatorial Pacific (Figure 27(b)). As with the MSLP signal, the SST anomaly field in the raw SST composite shows the dominance of the LF band La Niña pattern in the Pacific (Figure 12(a)). As in the austral autumn (boreal spring) of the El Niño sequences, there is evidence of SST dipole patterns over the Indian Ocean, on the QB band in this case (Figure 27(b)).

For the JAS season, La Niña characteristics are far more evident and show greater coherency across the entire domain. As witnessed during the previous seasons of this sequence, the LF band continues to carry the bulk of the La Niña signal in the MSLP field (Figure 28(c)). In addition, the QB band contributes through the positive MSLP anomaly over the Pacific Ocean Basin (Figure 28(a)). The SST anomaly patterns on the QB and, particularly, LF bands show a reinforcement of La Niña conditions across the Pacific Ocean in particular (Figure 28(b and d)), and provide the impetus for a strengthening of the raw SST signal in this season (Figure 13(a)). Once again, SST dipole patterns are evident over the Indian Ocean in each of the QB and LF SST anomaly fields, but slightly contrary spatial alignments on these bands lead to a less clear picture in the raw SST composite (Figure 13(a)). There is some suggestion on the LF band of a SST pattern containing the dipole of Chambers *et al.* (1999), Saji *et al.* (1999) and Webster *et al.* (1999), but with the reversed SST anomalies in western and eastern Indian Ocean nodes.

The final season in the La Niña-1 sequence, OND, sees the strong and coherent MSLP dipole pattern in the raw data (Figure 10(d)) carried mainly on the LF MSLP band (Figure 29(c)). There is some support from the QB band, but the signal is much reduced in magnitude when compared with that on the LF band (Figure 29(a and c)). A similar situation applies with regard to the raw SST composite (Figure 14(a)), which receives the bulk of its pattern from the dominant LF band across the entire Indo-Pacific domain (Figure 29(b and d)). During this season, both bands show some evidence of an eastern Indian Ocean SST dipole, as well as a strong north–south SST dipole, linked to the La Niña over the western and central Indian Ocean on the LF band (Figure 29(d)), but a less coherent pattern in the QB. As a result, the superposition of these bands is enough to bring up an eastern Indian Ocean dipole in the raw SST composite (Figure 14(a)), and highlights the fine balance in the system with regard to the contributions that significant signals make to the net result.

Overall, the La Niña-1 sequence showing the evolution towards the mature stage of the event is strongly dominated by fluctuations in MSLP and SST anomalies occurring on the LF band. Unlike the El Niño-1 sequence discussed earlier, the QB band is noticeably weaker in its contribution to the La Niña signal, in either MSLP or SST anomalies. This situation may explain why various studies have found evidence that the El Niño phase of ENSO is more robust and dominant when it occurs than is the La Niña. With SST dipole patterns in the Indian Ocean, there is evidence of their importance at various times during the La

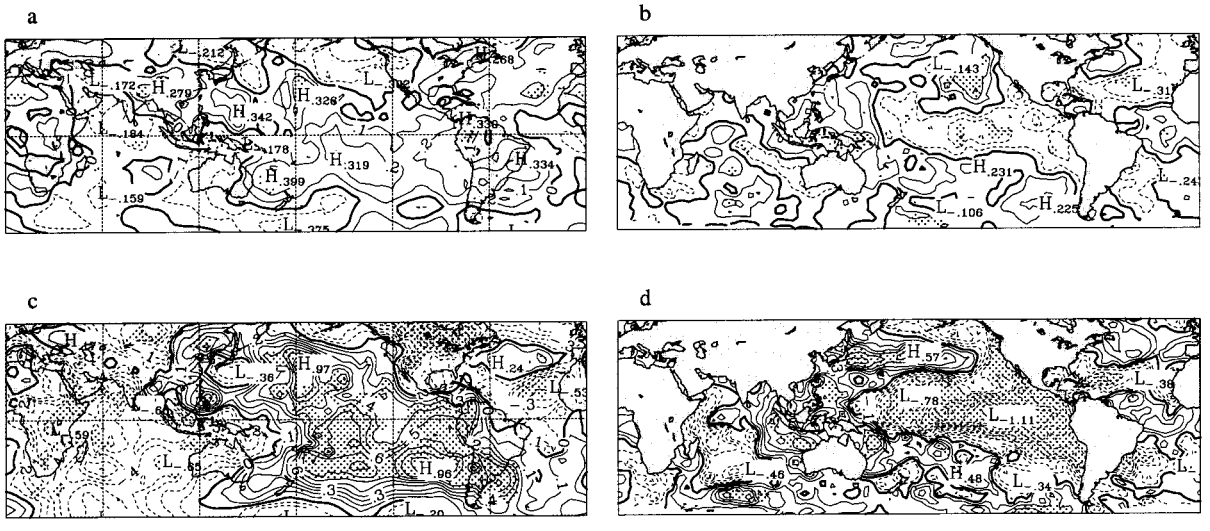

Figure 28. As in Figure 26, except for JAS season

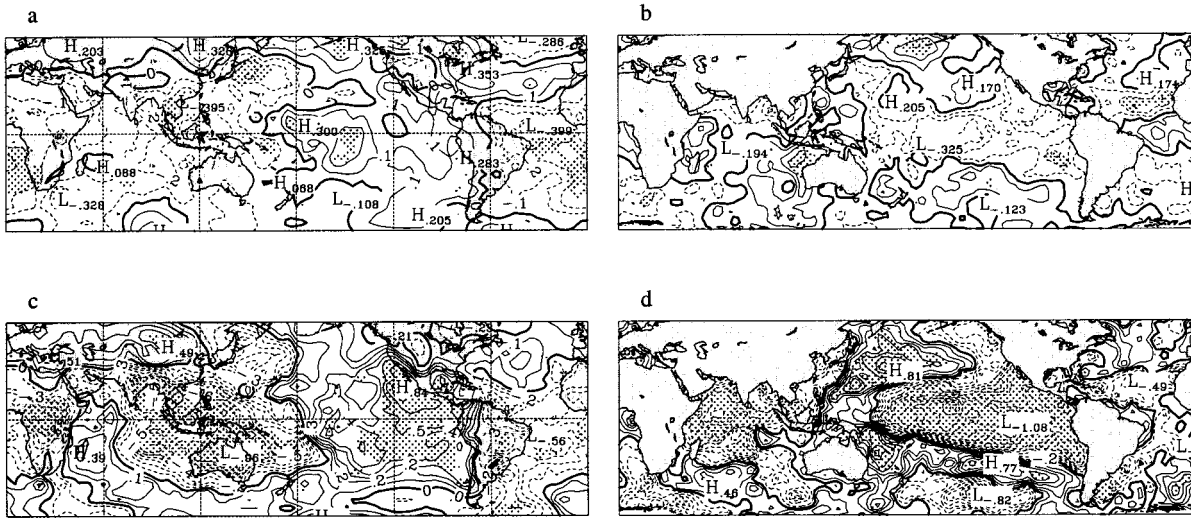

Figure 29. As in Figure 26, except for OND season

Niña-1 sequence, although they are perhaps not as pronounced during the austral autumn (boreal spring) season as they are in the El Niño-1 evolution.

4.4. La Niña

This sequence begins in the JFM season when the La Niña event across the Indo-Pacific domain is seen to reach its mature phase. In the MSLP anomaly fields, this can clearly be seen in the LF band (Figure 30(c)) where the bulk of the contribution to the raw MSLP field in Figure 15(a) is found. As in the La Niña-1 sequence, the QB band provides weaker support to the overall La Niña signal (Figure 30(a)). With SST anomalies, the QB signal shows a similar pattern (but weaker in magnitude) to that on the LF band, and both contribute to the raw SST signal (Figure 30(b and d) and Figure 16(a)). At this time, the strong La Niña signal in SST is most evident, with a pronounced north–south dipole over the central–western Indian Ocean being prominent on both bands. A weak SST dipole is also seen over the eastern portion of the Indian Ocean (Figure 30(b and d)).

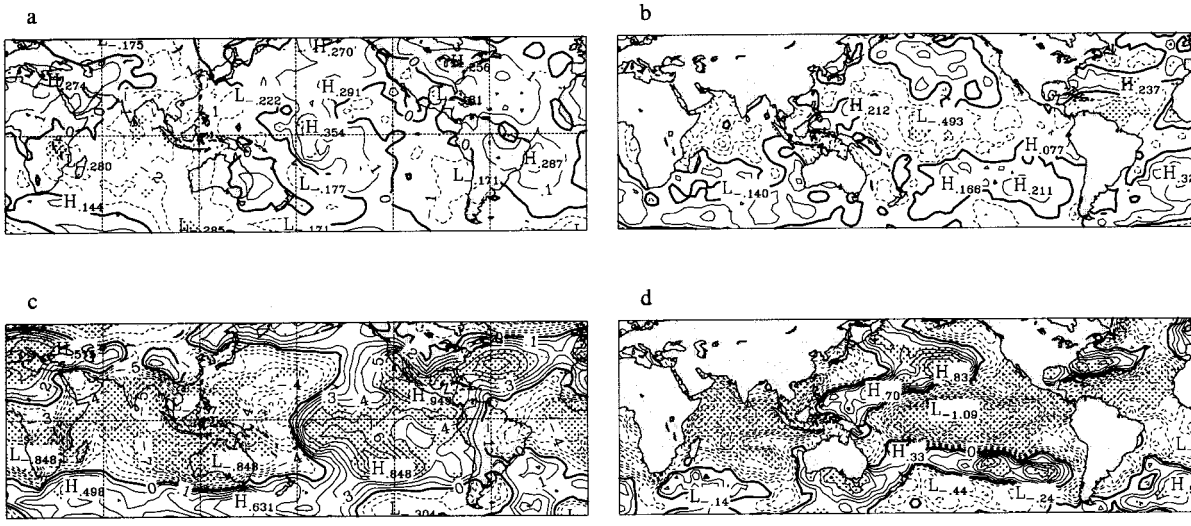

Figure 30. As in Figure 18, except showing La Niña composite sequence

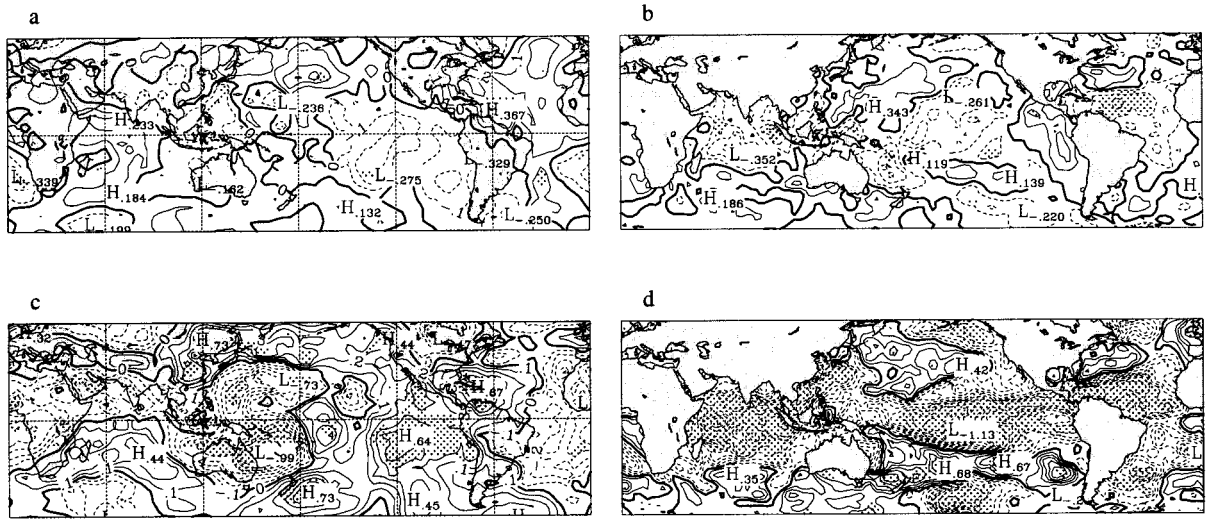

Figure 31. As in Figure 30, except for AMJ season

By the AMJ season, the La Niña signal begins to show signs of waning. The MSLP La Niña signal continues to be most strongly manifest on the LF band (Figure 31(c)), with a very fragmented picture of MSLP on the QB band (Figure 31(a)). As in the previous season, the raw MSLP signal (Figure 15(b)) is strongly modulated by the MSLP pattern on the LF band. The SST signal is once again mainly carried by the LF band over the Pacific (Figure 31(d)), but there appears to be a more equal contribution to the raw SST pattern over the Indian Ocean from both bands (Figure 17(a) and Figure 31(b and d)). This is the one austral autumn (boreal spring) composite in which there is poor definition of an SST dipole over the eastern portion of the Indian Ocean basin in either band (Figure 31(b and d)).

La Niña conditions continue to wane during the JAS composite, with the remaining signal of the MSLP dipole across the Indo-Pacific region being carried on the LF band (Figure 32(c)). Interestingly, the QB band MSLP anomaly pattern is beginning to show a structure not unlike a weak El Niño event (Figure 32(a)). Nevertheless, the major contribution to the raw MSLP signal continues to come primarily from the LF band (Figure 15(c) and Figure 32(a and c)). With SSTs, the situation is similar to that with MSLP on

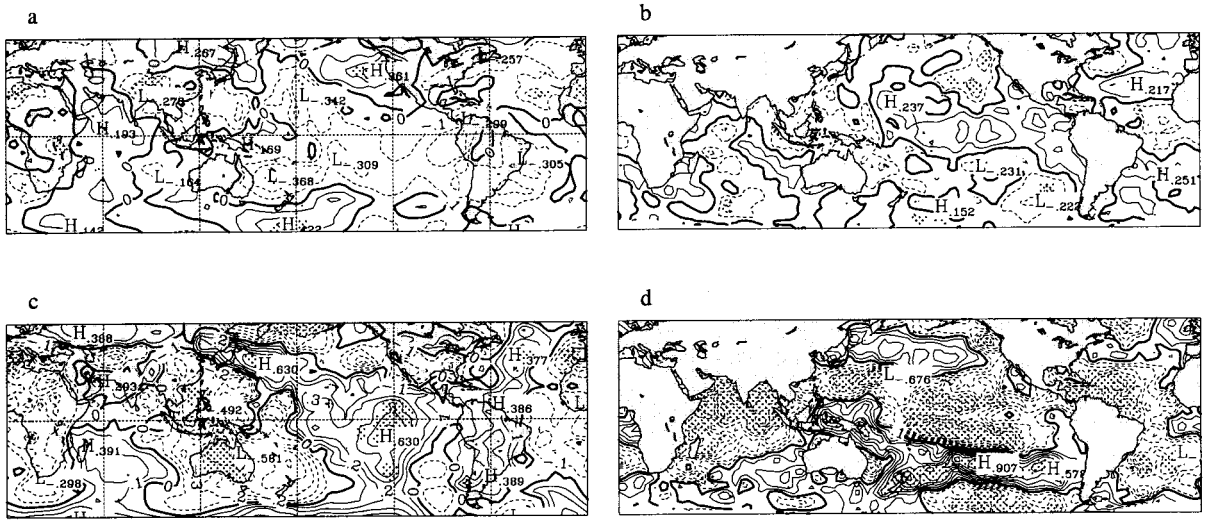

Figure 32. As in Figure 30, except for JAS season

the QB and LF bands. The bulk of the raw SST pattern (not shown) is found on the LF SST band (Figure 32(d)), with an SST pattern indicative of weak El Niño conditions across the central–eastern equatorial Pacific on the QB SST band (Figure 32(b)). In the Indian Ocean, there are distinct SST dipole patterns over the eastern portions of the basin on both QB and LF bands, with the former also tending to show a weak SST dipole in the western Indian Ocean (Figure 32(b and d)). However, none of these dipoles in SST is evident in the raw SST field during this season (not shown), as a result of the different spatial locations of these in the QB and LF bands.

The final season in the sequence, OND, sees the LF MSLP band anomaly again carrying the bulk of the raw MSLP signal over the Pacific (Figure 15(d) and Figure 33(a and c)). Although continuing to wane, a La Niña signal is still evident, but the QB band now has MSLP anomalies indicative of a dipole in the negative SOI phase (Figure 33(a)). Given the strong ocean–atmosphere coupling in the system, SST anomaly patterns on the QB and LF bands reflect the structures observed in the MSLP composites. The raw SST pattern (not shown) continues to show a persistence of weak La Niña conditions, but over the Pacific Ocean this is coming almost exclusively from the LF band (Figure 33(d)). As in the previous season, El Niño conditions are favoured over the Pacific on the QB SST band (Figure 33(b)). The persistence of a weak north–south SST dipole in the La Niña configuration over the Indian Ocean in the raw SST anomaly field (not shown), comes from the QB (LF) band in the western (eastern) portion of the basin (Figure 33(b and d)). In the tropical eastern south Indian Ocean, the LF SST band (Figure 33(d)) shows the strongest realization of an SST dipole, but this is greatly reduced by the QB band anomalies, so that little evidence of a dipole exists in the raw data (not shown).

In summary, the waning of the La Niña conditions across the equatorial Pacific in this sequence is most evident on the QB band in both MSLP and SST anomalies. In fact, the JAS and OND composites show a distinct shift to El Niño conditions in both fields on the QB band. Interestingly, the weakening of the La Niña event discussed above is far less advanced over the course of this sequence than was seen earlier for the El Niño event during its comparative sequence. Over the Indian Ocean, the La Niña conditions given by the north–south SST dipole show a tendency to be more evenly supported by both the QB and LF bands. Distinct SST dipoles over the eastern portion of the Indian Ocean Basin are most evident in the JAS composite, but in all cases are best resolved in these band pass filtered examinations of the raw data that reveal the QB and LF bands as separate entities.

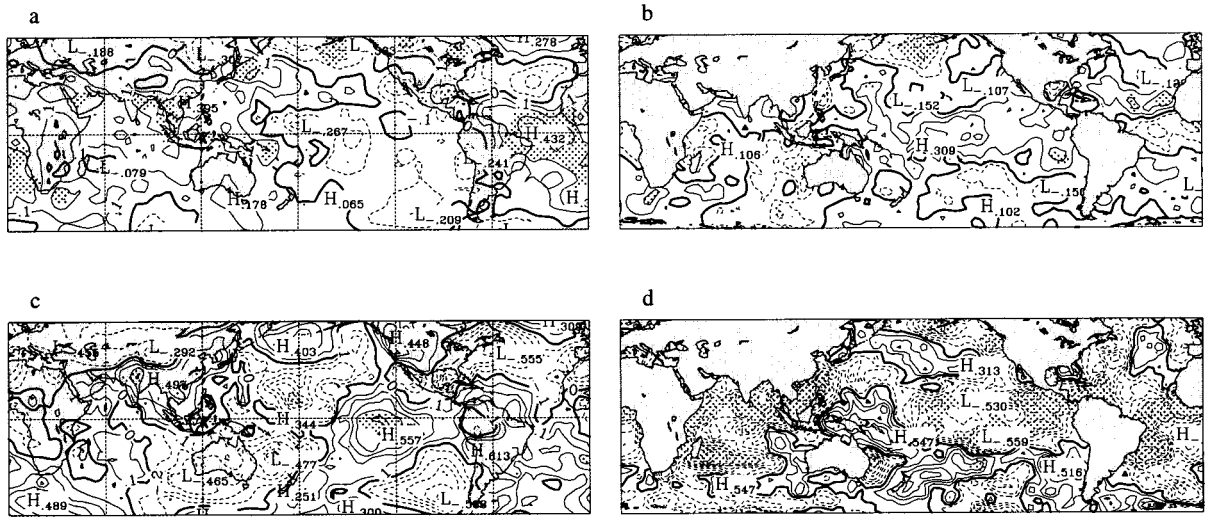

Figure 33. As in Figure 30, except for OND season

5. ENSO–RAINFALL CORRELATIONS IN THE QB AND LF BANDS

5.1. Interannual QB and LF ENSO

Global patterns of significant, simultaneous seasonal correlations between QB and LF joint MSLP and SST EOF time series from Hulme (1992) and Allan (2000) raw rainfall data are shown in Figure 34(a and b). These correlations reveal a pattern that reflects the well documented ENSO-sensitive regions on interannual time scales. However, several interesting aspects of these relationships over the Indian Ocean region are found, when rainfall correlations on the QB and LF bands are examined separately. In fact, the physical basis for the various rainfall correlation responses are evident, not only in the spatial components of the seasonal EOF patterns linked to the study of Allan (2000), but also in the MSLP and SST fields of the El Niño-1, El Niño, La Niña-1, and La Niña composites detailed in Section 4. Thus, not only oceanic temperature fields can be assessed, but also atmospheric circulation and general flow from an inspection of MSLP gradients.

Over southern Africa, the ENSO response in JFM (mature season) is strongest on the QB band (Figure 34(a)) and is reinforced by the relatively weaker response of the LF pattern (Figure 34(b)). Such a structure is consistent with previous work aimed at understanding the role of the stratospheric QB Oscillation in modulating ENSO influences over that part of the African continent (Mason and Tyson, 1992; Mason and Lindesay, 1993; Jury *et al.*, 1994; Mason, 1995). Southern African rainfall influences during the JFM season can be deduced from the corresponding mature phase El Niño and La Niña QB and LF composites of MSLP and SST anomalies in Figure 22(a–d) and Figure 30(a–d). On both bands, it is the combination of SST and circulation anomalies across southern Africa and the adjacent western Indian Ocean region that dictates the rainfall situation. During El Niño (La Niña) events on the QB band, more meridional south–southwesterly (east–southeasterly) flow anomalies across the region are directed over cooler (warmer) SSTs in the surrounding Atlantic and Indian Ocean waters, and thus bring dry (moist) conditions to southern Africa. This results in a stronger rainfall response in the region than occurs as a consequence of patterns on the LF band, where El Niño (La Niña) events are marked by strong, and more zonal west–southwesterly (easterly) wind anomalies directed over warmer (cooler) SST anomalies in the surrounding Atlantic and Indian Ocean waters, and thus bring less distinct rainfall conditions to southern Africa.

In the East African and Sri Lankan regions, peak ENSO signals occur during the OND season in both QB and LF rainfall correlations (Hastenrath *et al.*, 1993). Over the latter area, the rainfall response is more evenly divided between the QB and LF bands. However, in East Africa, the principal rainfall response tends to be found most strongly on the QB band. This is supported by the MSLP and SST anomaly fields during OND (Figure 21(a–d) and Figure 29(a–d)), where the QB band shows that during El Niño (La Niña) events more zonal easterly (westerly) flow anomalies over the central Indian Ocean (across East Africa) direct winds towards (away from) the region and across generally warm SST anomalies, and, thus, enhance (suppress) rainfall production. On the LF band during El Niño (La Niña) events, there are substantial positive (negative) pressure anomalies, which would tend to suppress (enhance) convection, and, therefore, provides less likelihood of increased (decreased) rainfall than on the QB band.

In the Sri Lankan region, the more even rainfall response on both bands (Suppiah, 1988) can be explained by reference to the MSLP and SST anomaly fields during the OND season in Figure 21(a–d) and Figure 29(a–d). During El Niño (La Niña) events on the QB and LF bands, stronger south–southeasterly (north–northwesterly) wind anomalies dominate in a region of warmer (cooler) SSTs over the northern Indian Ocean, and the Sri Lankan rainfall regime is enhanced (suppressed).

Across two of the prime ENSO-sensitive areas of the globe in India and northern–eastern Australia, the balance between QB and LF bands is variable, and either signal can play an important role in regional ENSO impacts. The Indian situation is most pronounced in JAS during the southwest summer monsoon (Figure 20(a–d) and Figure 28(a–d)). During strong El Niño (La Niña) events over India on the QB

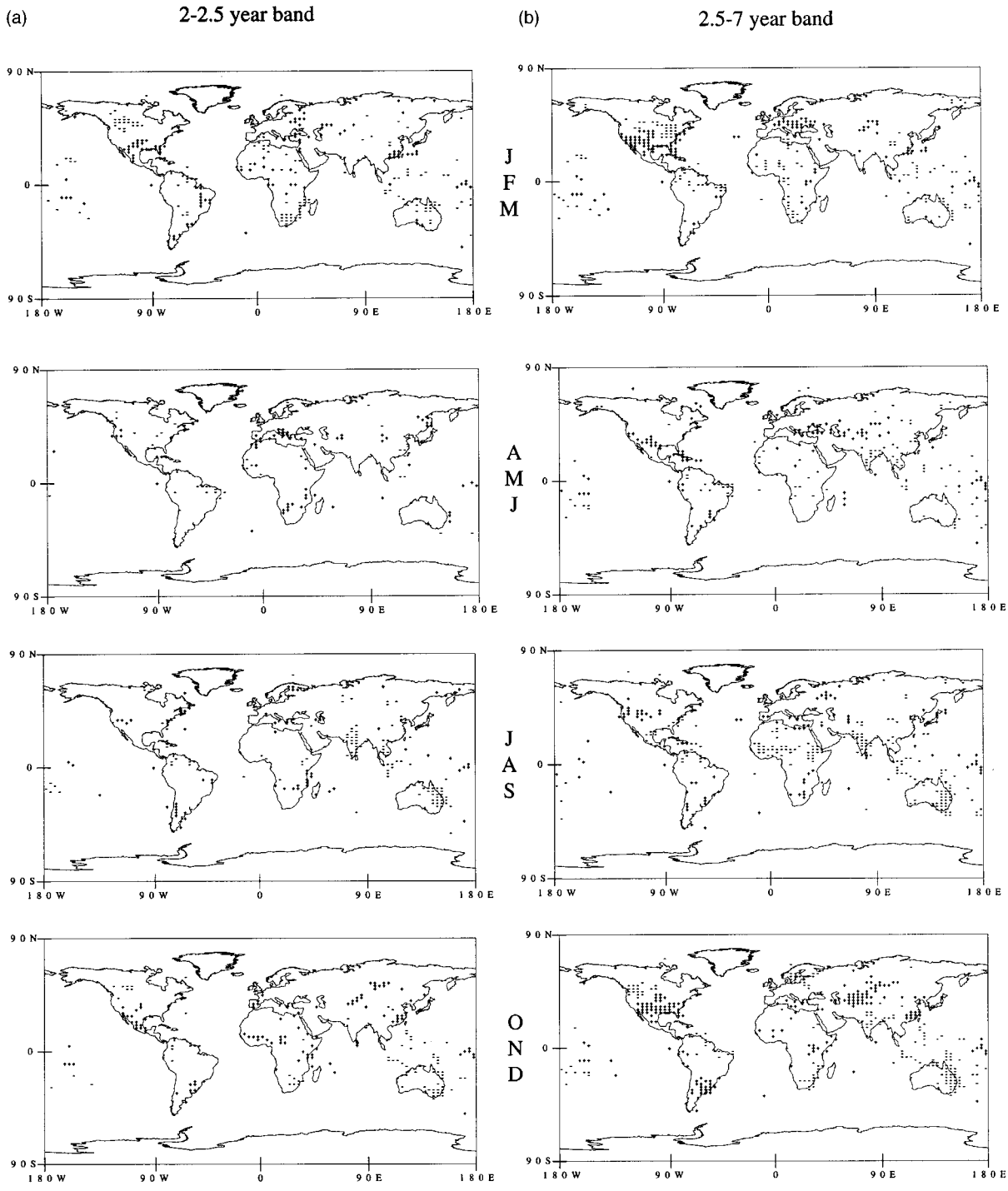

Figure 34. Global maps of statistically significant seasonal correlations between the joint EOF 1 time series and land, plus island raw precipitation data from Hulme (1992) in (a) the 2–2.5-year band, and (b) in the 2.5–7-year band for the period of 1900–1994. Positive and negative correlations that are statistically significant at the 95% level are indicated by the plus and minus signs, respectively. After Allan (2000)

band, the southwest monsoon flow tends to be suppressed (enhanced) and SSTs are cooler over the Arabian Sea and the Bay of Bengal (warmer in the Bay of Bengal) with lower (higher) rainfall.

The principal rainfall responses on the QB and LF bands over northern–eastern Australia are evident during the JAS, OND and JFM seasons. In the AMJ austral autumn (boreal spring) season of 'spring frailty', or the time of the 'predictability barrier', the least robust correlation patterns of any season in both the QB and LF bands are found. For the JFM season, the QB band rainfall correlation pattern shows a more significant and coherent response over the northern Australia region than the LF band (Figure 34(a and b)). This can be explained dynamically, in that on the QB band during El Niño (La Niña) events west–southwesterly (northerly) wind anomalies dominate, and flow is directed across northern Australia with warmer (cooler) SSTs in the surrounding waters (Figure 22(a and b) and Figure 30(a and b)). On the LF band in El Niño (La Niña) events, the very strong high (low) MSLP anomalies would tend to suppress (enhance) convection with monsoonal winds flowing over warmer (generally cooler) SSTs (Figure 22(c and d) and Figure 30(c and d)). Such responses with SSTs on both bands occur because northern Australian air–sea interactions at this time are such that a strengthening (weakening) of the prevailing monsoonal flow over warmer SSTs leads to the destruction (maintenance) of the oceanic temperature anomaly (Allan and Pariwono, 1990). Overall, the QB band has a more organized circulation and SST anomaly structure than the LF and produces a more distinct rainfall response at this time.

During JAS, eastern Australian rainfall correlation patterns in the QB band are most coherent over the northeast of the continent, while for the LF band, the more robust rainfall response is in the southeast. Examination of MSLP and SST anomaly fields (Figure 20(a–d) and Figure 28(a–d)) show that for the QB band, El Niño (La Niña) events are marked by west–southwesterly (northeast–northerly) wind flow directed away from (towards) northeastern Australia towards (across) cool (warm) SSTs in the Coral Sea. There is also a propensity during La Niña episodes on the QB band for enhanced eastern Indian Ocean dipole patterns in the configuration, most likely to aid in the development of tropical-temperate cloud bands directed towards northeastern to eastern Australia. For southeastern Australia, the LF band rainfall correlations during El Niño (La Niña) events are influenced by south–southwesterly (northeasterly) wind flow, directed over land from cool SSTs west of Western Australia (over warm SSTs in the Coral Sea) and an eastern Indian Ocean SST dipole conducive to suppressing (generating) tropical-temperate cloud bands and reduced (enhanced) rainfall producing systems.

For OND over Australia, the QB band shows most coherent rainfall correlations in northern and southeastern Australia, while the LF band displays a north–northeastern rainfall response. The dynamical features explaining the rainfall pattern on both bands can be seen in Figure 21(a–d) and Figure 29(a–d). On both bands, the northern Australian rainfall response is linked to El Niño (La Niña) events through high (low) MSLP anomalies, suppressing (enhancing) convection associated with flow coming from cooler Coral and Indonesian seas (warmer Indonesian seas). There is some evidence in the LF band of an eastern Indian Ocean SST dipole, which would tend to be conducive to the formation of tropical-temperate cloud bands, and, therefore, may be linked to the rainfall response over southeastern Australia.

6. CONCLUSION AND DISCUSSION

In this study, climatic signals have been isolated at various stages in the evolution of El Niño and La Niña events over the Indian Ocean Basin, in the context of the wider ENSO response across the Indo-Pacific domain. The resolution of raw and dominant QB and LF signals in seasonal composite sequences for both phases of the ENSO phenomenon, and the construction of seasonal rainfall correlations with QB and LF band joint MSLP and SST EOF time series, provides the basis for a detailed examination of ENSO structure, characteristics, dynamics and impacts, as they affect the Indian Ocean region.

Seasonal composites of raw MSLP, SST, wind and cloudiness anomalies over the full Indo-Pacific domain during El Niño-1, El Niño, La Niña-1, and La Niña sequences suggest that both phases of the ENSO phenomenon reach maturity during the JFM season after onset in the previous El Niño-1 or La Niña-1 year. In general, the composite El Niño-1 sequence tends to display a more robust and coherent

structure throughout the seasons leading up to the mature stage of the event than is seen with the La Niña-1 event sequence. For the cessation period after the mature stage, the reverse tends to occur, with the La Niña sequence showing a much longer persistence of that phase than is seen for the El Niño composite where the event has collapsed by the JAS season. The above characteristics may be modulating the non-linearity of near-global teleconnection patterns during ENSO phases noted by Hoerling *et al.* (1997).

Over the Indian Ocean Basin, the evolution of climatic variables during ENSO phases in the raw data is more or less simultaneous, except for the Indonesian region, where features are found to have a lag of about one season. An examination of the raw composites also suggests that SST may evolve in response to changes in cloud cover and wind strength over both the north and south Indian Ocean (presumably via changes to the surface latent and sensible heat fluxes and upper ocean mixing driven by atmospheric variations). As in the Pacific Ocean, modulations of the Walker circulation are evident over the African/Indian Ocean region (Allan *et al.*, 1996). The mature stage of both ENSO phases, during JFM of the El Niño and La Niña sequences, also marks a peak in Walker circulation changes. During El Niño (La Niña) events at this time, enhanced (reduced) cloudiness and convective activity tends to found in the western–central Indian Ocean east of Madagascar. Dynamical support for such changes is seen through regional fluctuations in westerly (easterly) wind anomalies off the northern tip of Madagascar that coincide with distinct warm–cool (cool–warm) patterns in the north–south SST dipole over the western Indian Ocean region during the El Niño (La Niña) event sequence. In addition, the raw SST composites in both ENSO phases suggest an eastern Indian Ocean SST dipole, particularly during the JAS and OND seasons of both the El Niño-1 and El Niño composites, and the AMJ, JAS and OND seasons of the La Niña-1 and JFM season of the La Niña composites.

Resolution of MSLP and SST anomaly patterns in the QB and LF bands, which together carry the bulk of the raw ENSO signal in these variables, in composite seasonal El Niño-1, El Niño, La Niña-1, and La Niña sequences, provides a finer resolution of the structure and nature of ENSO phases. Across the Indo-Pacific domain as a whole, this analysis reveals that the QB and LF contribution to the raw patterns of MSLP and SST signals is more consistent during the El Niño-1 and El Niño sequences than is found during the La Niña-1, and La Niña sequences. In fact, the QB band has generally less distinct, and in some cases, earlier or later in the sequences, the opposite anomaly patterns to that seen on the LF band. An example of the former case is during the La Niña-1 sequence where the LF band in both MSLP and SST is clearly the dominant source of the anomaly signal. The latter situation is particularly evident with regard to the El Niño composite during the cessation of the event, where the QB band carries a La Niña signal immediately after the JFM mature phase in both MSLP and SST anomalies. As a consequence, El Niño events are prone to be reinforced by both the QB and LF bands up to their mature phase, and then are eroded away rapidly during their cessation phase by the presence of distinct La Niña anomalies on the QB band. There is a tendency for the opposite configuration to occur during La Niña events, particularly with regard to their cessation phase.

Over the Indian Ocean, the analysis of QB and LF bands reveals important aspects of SST dipole patterns. In particular, it is evident that both bands often carry SST dipole anomalies, but as they are not always aligned spatially, any superposition of the patterns results in the dipoles being annulled, and, thus, being absent or very weakly defined in the raw composites. However, given that QB and LF signals are not always in phase, it then becomes highly likely that the SST dipole in the dominant band becomes well manifest and able to modulate the climate system in this region. This appears to be especially important for the eastern Indian Ocean SST dipole pattern, to the extent that during the austral autumn–winter (boreal spring–summer), when such SSTs can be best linked to tropical-temperate cloud bands influencing Australian rainfall patterns, QB and LF dipoles are found to occur, but are not closely aligned in their patterns. Thus, the raw SST patterns across the Indian Ocean at this time show little evidence of the eastern dipole, particularly during El Niño events when this mismatching appears to be most prevalent. As a consequence, eastern Indian Ocean SST dipole patterns are likely to be manifest during the onset phase of particular El Niño episodes, when either the QB or LF band is dominant. This is particularly true for the SST dipole pattern of Chambers *et al.* (1999), Saji *et al.* (1999) and Webster *et al.* (1999), which is clearly evident in the composites detailed in this study.

An examination of correlations between joint MSLP and SST EOF time series and raw rainfall data from countries bordering the Indian Ocean Basin, and the dynamical relationship with MSLP and SST anomalies during El Niño and La Niña events on QB and LF bands, shows that the correlation patterns can be linked to physically consistent ocean–atmosphere interactions. In general, it is the interplay between atmospheric circulation and SST anomalies in the different regional contexts that dictate the rainfall response during El Niño and La Niña episodes. In many instances, this involves both QB and LF modulations of rainfall regimes, although several regions show a marked QB influence over that provided by the LF band. This behaviour extends to the El Niño and La Niña influence on the Indo-Pacific domain, and highlights the fact that a much better understanding of the ENSO phenomenon and its impacts can be gained by examining the effect of its dominant QB and LF signals, rather than the usual focus on the overall raw indices and patterns. The prime example of the benefits of the above approach is seen with regard to eastern Indian Ocean SST dipole patterns. These features are usually smeared in raw analyses or composites, but their influence becomes apparent at times during El Niño or La Niña events, when either QB or LF band SST anomalies prevail, and the Indian Ocean can provide a different modulation on Australian rainfall patterns than that which is usually seen when that ocean is in phase with ENSO episodes in the Pacific.

A second, complementary paper is being prepared that will expand on the analyses and findings in this study by focusing on interactions between decadal and multidecadal climatic variability and ENSO signals across the Indian Ocean Basin.

ACKNOWLEDGEMENTS

Partial funding from the Australian Research Council (ARC) is gratefully acknowledged. Dr R.J. Allan is supported jointly through the CSIRO 'Climate Variability and Impacts Programme', and 'Climate Change and Impacts Programme', and funded in part by the Australian Federal Government's National Greenhouse Research Programme of the Australian Greenhouse Office, and the State Government of Queensland. We are grateful to Tony Fisher, who made his Chebychev filter program available to us, and to Kevin Keay for advice in its application. Peter Otto assisted with preparation of some of the diagrams.

REFERENCES

Allan RJ. 2000. ENSO and climatic variability in the last 150 years. In *El Niño and the Southern Oscillation: Multiscale Variability and its Impacts on Natural Ecosystems and Society*, Diaz HF, Markgraf V (eds). Cambridge University Press: Cambridge, UK (in press).

Allan RJ, Pariwono JI. 1990. Ocean–atmosphere interactions in low latitude Australasia. *International Journal of Climatology* **10**: 145–178.

Allan RJ, D'Arrigo RD. 1999. 'Persistent' ENSO sequences: how unusual was the 1990–1995 El Niño? *The Holocene* **9**: 101–118.

Allan RJ, Lindesay JA, Parker DE. 1996. *El Niño–Southern Oscillation and Climatic Variability*. CSIRO Publishing: Collingwood, Victoria.

Allan RJ, Lindesay JA, Reason CJC. 1995. Multidecadal variability in the climate system over the Indian Ocean region during the austral summer. *Journal of Climate* **8**: 1853–1873.

Basnett TA, Parker DE. 1997. Development of the Global Mean Sea Level pressure data set GMSLP2. Climate Research Technical Note CRTN79, Hadley Centre, Meteorological Office, Bracknell, UK.

Cadet DL. 1985. The Southern Oscillation over the Indian Ocean. *Journal of Climatology* **5**: 189–212.

Chambers DP, Tapley BD, Stewart RH. 1999. Anomalous warming in the Indian Ocean coincident with El Niño. *Journal of Geophysical Research* **104**: 3035–3047.

Clarke AJ, Liu X. 1994. Interannual sea level in the northern and eastern Indian Ocean. *Journal of Physical Oceanography* **24**: 1224–1235.

Clarke AJ, Liu X, van Gorder S. 1998. Dynamics of the Biennial Oscillation in the equatorial Indian and far western Pacific Oceans. *Journal of Climate* **11**: 987–1001.

Drosdowsky W. 1993a. An analysis of Australian seasonal rainfall anomalies: 1950–1987. II: Temporal variability and teleconnection patterns. *International Journal of Climatology* **13**: 111–149.

Drosdowsky W. 1993b. Potential predictability of winter rainfall over southern and eastern Australia using Indian Ocean sea-surface temperature anomalies. *Australian Meteorological Magazine* **42**: 1–6.

Folland CK, Parker DE, Colman AW, Washington R. 1998. Large scale modes of ocean surface temperature since the late nineteenth century. Climate Research Technical Note CRTN81, Hadley Centre, Meteorological Office, Bracknell, UK.

Fu C, Fletcher J. 1988. Large signals of climatic variation over the ocean in the Asian monsoon region. *Advanced Atmospheric Science* **5**: 389–404.

Godfrey JS, Alexiou A, Ilahude AG, Legler DM, Luther ME, McCready JP Jr, Meyers GA, Mizumo K, Rao RR, Shetye SR, Toole JH, Wacongne S. 1995. The role of the Indian Ocean in the Global Climate System: recommendations regarding the global ocean observing system. Report of the Ocean Observing System Development Panel (OOSDP), Report No. 6, Texas A&M University, College Station, Texas.

Graham NE. 1994. Decadal-scale climate variability in the tropical and North Pacific during the 1970s and 1980s: observations and model results. *Climate Dynamics* **10**: 135–162.

Halpert MS, Ropelewski CF. 1992. Surface temperature patterns associated with the Southern Oscillation. *Journal of Climate* **5**: 577–593.

Hantel M. 1970. Monthly charts of surface wind vergence over the tropical Indian Ocean. *Bonner Meteorolgische Abhandlungen* **14**: 31–79.

Harrison DE, Larkin NK. 1996. The COADS sea level pressure signal: a near-global El Niño composite and time series view, 1946–1993. *Journal of Climate* **9**: 3025–3055.

Hastenrath S, Nicklis A, Greischar L. 1993. Atmospheric–hydrospheric mechanisms of climate anomalies in the western equatorial Indian Ocean. *Journal of Geophysical Research* **98**: 219–220 (see also pp. 20, 235).

Hirst AC, Godfrey JS. 1993. The role of the Indonesian throughflow in a global ocean GCM. *Journal of Physical Oceanography* **23**: 1057–1086.

Hirst AC, Godfrey JS. 1994. The response to a sudden change in Indonesian throughflow in a global ocean GCM. *Journal of Physical Oceanography* **24**: 1895–1910.

Hoerling MP, Kumar A, Zhong M. 1997. El Niño, La Niña and the nonlinearity of their teleconnections. *Journal of Climate* **10**: 1769–1786.

Hulme M. 1992. A 1951–1980 global land precipitation climatology for the evaluation of general circulation models. *Climate Dynamics* **7**: 57–72.

Hulme M, New M. 1997. Dependence of large-scale precipitation climatologies on temporal and spatial sampling. *Journal of Climate* **10**: 1099–1113.

Hutchinson P. 1992. The Southern Oscillation and the prediction of 'Der' season rainfall in Somalia. *Journal of Climate* **5**: 525–531.

Janowiak J. 1988. An investigation of interannual variability in Africa. *Journal of Climate* **1**: 240–255.

Jiang F-F, Neelin JD, Ghil M. 1995. Quasi-quadrennial and quasi-biennial variability in the equatorial Pacific. *Climate Dynamics* **12**: 101–112.

Jury MR. 1994. Regional teleconnection patterns associated with summer rainfall over South Africa, Namibia and Zimbabwe. *International Journal of Climatology* **16**: 135–153.

Jury MR, Valentine HR, Lutjeharms JRE. 1993. Influence of the Agulhas Current on summer rainfall on the southeast coast of South Africa. *Journal of Applied Meteorology* **32**: 1282–1287.

Jury MR, McQueen C, Levy KM. 1994. SOI and QBO signals in the African region. *Theoretical and Applied Climatology* **50**: 103–115.

Jury MR, Pathack B, de W. Rautenbach CJ, van Heerden J. 1996. Drought over South Africa and Indian Ocean SST: statistical and GCM results. *The Global Atmosphere and Ocean System* **4**: 47–63.

Kerr RA. 1994. Did the tropical Pacific drive the world's warming? *Science* **266**: 544–545.

Kiladis GN, Diaz HF. 1989. Global climatic anomalies associated with extremes in the Southern Oscillation. *Journal of Climate* **2**: 1069–1090.

Kleeman R, Colman RA, Smith NR, Power SB. 1996. A recent change in the mean state of the Pacific Basin: observational evidence and atmospheric and oceanic responses. *Journal of Geophysical Research* **101**: 20 483–20 499.

Kripalani RH, Kulkarni A. 1997a. Rainfall variability over southeast Asia—connections with Indian monsoon and ENSO extremes: new perspectives. *International Journal of Climatology* **17**: 1155–1168.

Kripalani RH, Kulkarni A. 1997b. Climatic impact of El Niño/La Niña on the Indian monsoon: a new perspective. *Weather* **52**: 39–46.

Kripalani RH, Kulkarni A. 1998. The relationship between some large-scale atmospheric parameters and rainfall over southeast Asia: a comparison with features over India. *Theoretical and Applied Climatology* **59**: 1–11.

Latif M, Kleeman R, Eckert C. 1997. Greenhouse warming, decadal variability, or El Niño? An attempt to understand the anomalous 1990s. *Journal of Climate* **10**: 2221–2239.

Latif M, Groetzner A, Barnett TP. 1996. A mechanism for decadal climate variability. *Atlantic Climate Change Program Notes* **3**: 1–3.

Lindesay JA. 1988. South African rainfall, the Southern Oscillation and a Southern Hemisphere semi-annual cycle. *Journal of Climatology* **8**: 17–30.

Lindesay JA, Harrison MSJ, Haffner MP. 1986. The Southern Oscillation and South African rainfall. *South African Journal of Science* **82**: 196–198.

Lindesay JA, Vogel CH. 1990. Historical evidence for Southern Oscillation–southern African rainfall relationships. *International Journal of Climatology* **10**: 679–689.

Makarau A, Jury MR. 1997. Predictability of Zimbabwe summer rainfall. *International Journal of Climatology* **17**: 1421–1432.

Mason SJ. 1990. Temporal variability of sea surface temperatures around Southern Africa: a possible forcing mechanism for the 18-year rainfall oscillation? *South African Journal of Science* **86**: 243–252.

Mason SJ. 1995. Sea-surface temperature–South African rainfall associations, 1910–1989. *International Journal of Climatology* **15**: 119–135.

Mason SJ, Lindesay JA. 1993. A note on the modulation of Southern Oscillation–southern African rainfall associations with the Quasi-biennial Oscillation. *Journal of Geophysical Research* **98**: 8847–8850.

Mason SJ, Tyson PD. 1992. The modulation of sea surface temperature and rainfall associations over southern Africa with solar activity and the Quasi-biennial Oscillation. *Journal of Geophysical Research* **97**: 5847–5856.

Matarira CH. 1990. Drought over Zimbabwe in a regional and global context. *International Journal of Climatology* **10**: 609–625.

Meyers G. 1996. Variation of Indonesian throughflow and the El Niño–Southern Oscillation. *Journal of Geophysical Research* **101**: 12255–12264.
Miller AJ, Cayan DR, Barnett TP, Graham NE, Oberhuber JM. 1994a. Interdecadal variability of the Pacific Ocean: model response to observed heat flux and wind stress anomalies. *Climate Dynamics* **9**: 287–302.
Miller AJ, Cayan DR, Barnett TP, Graham NE, Oberhuber JM. 1994b. The 1976-77 climate shift of the Pacific Ocean. *Oceanography* **7**: 21–26.
Nicholls N. 1989. Sea surface temperatures and Australian winter rainfall. *Journal of Climate* **2**: 965–973.
Nicholson SE. 1997. An analysis of the ENSO signal in the tropical Atlantic and western Indian Oceans. *International Journal of Climatology* **17**: 345–375.
Nicholson SE, Entekhabi O. 1986. Quasi-periodic behaviour of rainfall variability in Africa. *Archives for Meteorology, Geophysics and Bioclimatology (Series A)* **34**: 311–348.
Nicholson SE, Palao I. 1993. A re-evaluation of rainfall variability in the Sahel, Part I. Characteristics of rainfall fluctuations. *International Journal of Climatology* **13**: 371–389.
Nicholson SE, Kim J. 1997. The relationship of the El Niño–Southern Oscillation to African rainfall. *International Journal of Climatology* **17**: 117–135.
Pan YH, Oort AH. 1990. Correlation analyses between sea surface temperature anomalies in the eastern equatorial Pacific and the world ocean. *Climate Dynamics* **4**: 191–205.
Parker DE, Jackson M, Horton EB. 1995. The GISST2.2 sea surface temperature and sea-ice climatology. Climate Research Technical Note CRTN63, Hadley Centre, Meteorological Office, Bracknell, UK.
Parthasarathy K, Kumar KR, Munot AA. 1991. Evidence of secular variations in Indian monsoon rainfall–circulation relationships. *Journal of Climate* **4**: 927–938.
Parthasarathy K, Kumar KR, Munot AA. 1992. Surface pressure and summer monsoon rainfall over India. *Advanced Atmospheric Science* **9**: 359–366.
Philander SGH. 1990. *El Niño, La Niña and the Southern Oscillation*. Academic Press: New York.
Qu T, Meyers G, Godfrey JS. 1994. Ocean dynamics in the region between Australia and Indonesia and its influence on the variation of sea surface temperature in a global general circulation model. *Journal of Geophysical Research* **99**: 18 433–18 445.
Rasmusson EM, Carpenter TH. 1982. Variations in tropical sea surface temperature and surface wind fields associated with the Southern Oscillation/El Niño. *Monthly Weather Review* **110**: 354–384.
Rayner NA, Horton EB, Parker DE, Folland CK, Hackett RB. 1996. Version 2.2 of the Global sea-Ice and Sea Surface Temperature data set, 1903–1994. Climate Research Technical Note CRTN74, Hadley Centre, Meteorological Office, Bracknell, UK.
Reason CJC. 1998. Warm and cold events in southeast Atlantic/southwest Indian Ocean region and potential impacts on circulation and rainfall over southern Africa. *Meteorology and Atmospheric Physics* **69**: 49–65.
Reason CJC. 1999. Interannual warm and cool events in the subtropical/midlatitude south Indian Ocean region. *Geophysical Research Letters* **26**: 215–218.
Reason CJC, Lutjeharms JRE. 1998. Variability of the south Indian Ocean and implications for southern African rainfall. *South African Journal of Science* **94**: 115–123.
Reason CJC, Allan RJ, Lindesay JA. 1996a. Dynamical response of the oceanic circulation and temperature to interdecadal variability in the surface winds over the Indian Ocean. *Journal of Climate* **9**: 97–114.
Reason CJC, Allan RJ, Lindesay JA. 1996b. Evidence for the influence of remote forcing on interdecadal variability in the southern Indian Ocean. *Journal of Geophysical Research* **101**: 11 867–11 882.
Reason CJC, Allan RJ, Lindesay JA. 1998a. Climate variability on decadal/interdecadal time scales: mechanisms and implications for climate change. *Palaeoclimates: Data and Modelling* **3**(1-3): 25–49.
Reason CJC, Godfred-Spenning CR, Allan RJ, Lindesay JA. 1998b. Air–sea interaction mechanisms and low frequency climate variability in the south Indian Ocean region. *International Journal of Climatology* **18**: 391–405.
Reverdin G, Cadet DL, Gutzler D. 1986. Interannual displacement of convection and surface circulation over the equatorial Indian Ocean. *Quarterly Journal of the Royal Meteorological Society* **112**: 43–67.
Rocha A, Simmonds IH. 1997a. Interannual variability of south-eastern African summer rainfall. Part I: Relationships with air–sea interaction processes. *International Journal of Climatology* **17**: 235–265.
Rocha A, Simmonds IH. 1997b. Interannual variability of southeastern African summer rainfall. Part II: Modelling the impact of sea surface temperatures on rainfall and circulation. *International Journal of Climatolology* **17**: 267–290.
Ropelewski CF, Halpert MS. 1987. Global and regional scale precipitation patterns associated with the El Niño–Southern Oscillation. *Monthly Weather Review* **115**: 1606–1626.
Ropelewski CF, Halpert MS. 1989. Precipitation patterns associated with the high index phase of Southern Oscillation. *Journal of Climate* **2**: 268–284.
Saji NH, Goswami BN, Vinayachandran PN, Yamagata T. 1999. A dipole mode in the tropical Indian Ocean. *Nature* **401**: 360–363.
Smith IN. 1994. Indian Ocean sea-surface temperature patterns and Australian winter rainfall. *International Journal of Climatology* **14**: 287–305.
Suppiah R. 1988. Atmospheric circulation variations and the rainfall of Sri Lanka. Science Reports of the Institute of Geophysics, University of Tsukuba, Section A, Vol. 9; 75–142.
Suppiah R. 1996. Spatial and temporal variations in the relationships between the Southern Oscillation phenomenon and rainfall of Sri Lanka. *International Journal of Climatology* **16**: 1391–1408.
Thapliyal V, Kulshrestha SM. 1991. Climate changes and trends over India. *Mausam* **42**: 333–338.
Torrence C, Compo GP. 1998. A practical guide to wavelet analysis. *Bulletin of the American Meteorological Society* **79**: 61–78.
Torrence C, Webster PJ. 1998. The annual cycle of persistence in the El Niño–Southern Oscillation. *Quarterly Journal of the Royal Meteorological Society* **124**: 1985–2004.
Torrence C, Webster PJ. 1999. Interdecadal changes in the ENSO–monsoon system. *Journal of Climate* **12**: 2679–2690.
Trenberth KE, Hurrell JW. 1994. Decadal atmosphere–ocean variations in the Pacific. *Climate Dynamics* **9**: 303–319.

Tyson PD. 1986. *Climatic Change and Variability in Southern Africa*. Oxford University Press: Cape Town, South Africa.
van Heerden J, Terblanche DE, Schulze G. 1988. The Southern Oscillation and South African summer rainfall. *International Journal of Climatology* **8**: 577–597.
Vijayakumar R, Kulkarni JR. 1995. The variability of the interannual oscillations of the Indian summer monsoon rainfall. *Advanced Atmospheric Science* **12**: 95–102.
Wajsowicz RC. 1994. A relationship between interannual variations in the South Pacific wind stress curl, the Indonesian Throughflow, and the West Pacific warm water pool. *Journal of Physical Oceanography* **24**: 2180–2187.
Wajsowicz RC. 1995. The response of the Indo-Pacific Throughflow to interannual variations in the Pacific wind stress. Part I, Idealized geometry and variations. *Journal of Physical Oceanography* **25**: 1805–1826.
Walker ND. 1990. Links between South African summer rainfall and temperature variability of the Agulhas and Benguela Current systems. *Journal of Geophysical Research* **95**: 3297–3319.
Walker ND, Lindesay JA. 1989. Preliminary observations of oceanic influences on the February–March 1988 floods in central South Africa. *South African Journal of Science* **85**: 164–169.
Webster PJ. 1995. The annual cycle and the predictability of the tropical coupled ocean–atmosphere system. *Meteorological and Atmospheric Physics* **56**: 33–55.
Webster PJ, Yang S. 1992. Monsoon and ENSO: Selectively interactive systems. *Quarterly Journal of the Royal Meteorological Society* **118**: 877–926.
Webster PJ, Moore AM, Loschnigg JP, Leben RR. 1999. Coupled ocean–atmosphere dynamics in the Indian Ocean during 1997–1998. *Nature* **401**: 356–360.
Wolter K. 1987. The Southern Oscillation in surface circulation and climate over the tropical Atlantic, eastern Pacific, and Indian Oceans as captured by cluster analysis. *Journal of Climate and Applied Meteorology* **26**: 540–558.
Wolter K. 1989. Modes of tropical circulation, Southern Oscillation, and Sahel rainfall anomalies. *Journal of Climate* **2**: 149–172.
Woodruff SD, Slutz RJ, Jenne RL, Steurer PM. 1987. A comprehensive ocean–atmosphere data set. *Bulletin of the American Meteorological Society* **68**: 1239–1250.
Wright PB, Mitchell TP, Wallace JM. 1985. Relationships between surface observations over the global oceans and the Southern Oscillation. NOAA Data Report ERL PMEL-12.
Wyrtki K. 1987. Indonesian Through Flow and the associated pressure gradient. *Journal of Geophysical Research* **92**: 12 941–12 946.

